ornl

ORNL/TM-10954

OAK RIDGE
NATIONAL
LABORATORY

MARTIN MARIETTA

Prospects For and Tests of Hadron Calorimetry with Silicon

James E. Brau
Tony A. Gabriel
P. G. Rancoita

OAK RIDGE NATIONAL LABORATORY
CENTRAL RESEARCH LIBRARY
CIRCULATION SECTION
4500N ROOM 175
LIBRARY LOAN COPY
DO NOT TRANSFER TO ANOTHER PERSON
If you wish someone else to see this report, send in name with report and the library will arrange a loan.

OPERATED BY
MARTIN MARIETTA ENERGY SYSTEMS, INC.
FOR THE UNITED STATES
DEPARTMENT OF ENERGY

[illegible]
National Technical Information Service
[illegible] Department of Commerce
5285 Port Royal Road, Springfield, Virginia 22161
NTIS price codes: Printed Copy [illegible] Microfiche [illegible]

This report was prepared as an account of work sponsored by an agency of the United States Government. Neither the United States Government nor any agency thereof, nor any of their employees, makes any warranty, express or implied, or assumes any legal liability or responsibility for the accuracy, completeness, or usefulness of any information, apparatus, product, or process disclosed, or represents that its use would not infringe privately owned rights. Reference herein to any specific commercial product, process, or service by trade name, trademark, manufacturer, or otherwise, does not necessarily constitute or imply its endorsement, [illegible] any agency thereof. [illegible] necessarily [illegible] thereof.

ORNL/TM-10954

Engineering Physics and Mathematics

Prospects For and Tests of Hadron Calorimetry with Silicon†

James E. Brau*
Tony A. Gabriel
P. G. Rancoita[ξ]

†Submitted for publication.

*Dept. of Physics, University of Oregon

[ξ]INFN, Milan, Italy

DATE PUBLISHED — March 1989

NOTICE: This document contains information of a preliminary nature. It is subject to revision or correction and therefore does not represent a final report.

Prepared by the
OAK RIDGE NATIONAL LABORATORY
Oak Ridge, Tennessee 37831
operated by
MARTIN MARIETTA ENERGY SYSTEMS, INC.
for the
U.S. DEPARTMENT OF ENERGY
under contract DE-AC05-84OR21400

MARTIN MARIETTA ENERGY SYSTEMS LIBRARIES

3 4456 0290544 4

CONTENTS

ABSTRACT v
1. INTRODUCTION 1
2. FUNDAMENTAL PHYSICS OF COMPENSATING CALORIMETERS . 3
2.1 BASIC IDEAS 3
2.2 BINDING ENERGY LOSSES 6
2.3 NEUTRONS 6
2.4 EARLY CALCULATIONS 14
2.5 HYDROGENOUS MEDIA 14
2.6 ELECTROMAGNETIC SAMPLING 16
3. CALCULATIONS OF SILICON HADRON CALORIMETERS . . . 20
4. EXPERIMENTAL TEST OF SI/U 28
5. DISCUSSION OF POTENTIAL LIMITATIONS 33
6. CONCLUSIONS 34
APPENDIX 35
REFERENCES 36

ABSTRACT

Hadron calorimetry with silicon may provide crucial capabilities in experiments at the high luminosity, high energy colliders of the future, particularly due to silicon's fast intrinsic speed and absolute calibration. The important underlying processes of our understanding of hadron calorimeters are reviewed to set the framework for the presentation of recent calculations of the expected performance of silicon detector based hadron calorimeters. Such devices employing uranium are expected to achieve the compensation condition (that is, the ratio of the most probable electron signal to hadron signal (e/h) is $\approx$ 1.0) based on the understanding that has been derived from the uranium-liquid argon and uranium-plastic scintillator systems. In fact, even lead-silicon calorimeters are found to achieve the attractive value for the e/h ratio of 1.16 at 10 GeV. An experimental test of these predictions is underway at CERN by the SICAPO Collaboration.

1. INTRODUCTION

The physics results of future high luminosity, high energy colliders (eg. SSC or LHC) will depend on having very good calorimeters, which have been designed and constructed using the latest state of the art techniques. Many reviews have summarized the existing knowledge of calorimeter physics.[1-4] However, the understanding of the fundamental processes which limit calorimeter performance has undergone a significant advancement in recent years. It will be crucial to apply this understanding in the best ways. The present understanding has evolved through an interchange between theoretical calculations and experimental test programs, as the conclusions drawn from the theory in the calculations have been tested and found to be fundamentally sound. In this paper we will apply this understanding to assess the prospects for hadronic calorimetry with silicon and report on the experimental test underway at CERN.

Four years ago a new understanding of the underlying mechanisms of compensating calorimetry was introduced.[5-10] At that time the following critical points were realized:

1. prior to later experimental confirmation, it was argued that current designs of uranium liquid argon calorimeters were not fully compensating[5-9];
2. the importance of the hydrogen content in the active medium to couple the low energy neutrons to the output signal was stressed[5-9];
3. the significant role of "electromagnetic sampling inefficiencies" (which are the result of preferential photon absorption[11] and electron multiple scattering in the high-Z inactive material[6,9]) in reducing the ratio of electron to hadron response was explained[5-9];
4. the importance of the saturation of signal in the regions of high density energy deposition was emphasized[5-9]; and
5. these new understandings led us to "predict that a lead calorimeter may also give EM/HAD ≈ 1 "[12], where EM/HAD is the ratio of average electron to hadron response for the same incident kinetic energy, hereafter referred to as the e/h ratio. In other words, a compensating lead calorimeter was predicted.

At the time this new understanding was introduced in 1984, it was not generally accepted and met with much scepticism in the community. As a result of much experimental testing in the past four years, this scepticism has evolved to a general acceptance by the community. Shortly after the new understanding of compensation was announced, the experimental test programs of D0 at Fermilab and SLD at SLAC presented new data which supported the partial compensation expected for uranium liquid argon calorimeters. The predictions of the Monte Carlo calculations agreed very well with the new measurements.[9] Furthermore, the interpretation of the fundamental processes driving this behaviour had been determined and was presented at that time. The understanding of the role of hydrogen was expanded with the introduction of a prediction by Brückmann[13] of "tuning" of relative electron and hadron response by varying the ratio of uranium plate thickness to the scintillator thickness. Test beam studies of uranium scintillator calorimeters have confirmed the expected trends from the model of "tuning".[14] Considerations of the role of "tuning" in non-uranium scintillator calorimeters led to a specific design of a lead-scintillator compensating calorimeter with the ratio of lead thickness to

scintillator thickness of approximately four; it was subsequently built and found to have e/h = 1.05 ± 0.04.[15] Recently an activation analysis[16] of calorimeter-like stacks at CERN has confirmed the details of neutron-hydrogen coupling[7,8] which were key to the new understanding of calorimetry introduced in 1984. This new understanding has now been generally accepted and serves as the foundation of recent reviews of the phenomenology of compensating calorimeters.[17,18]

The challenge of doing physics at the next generation hadron colliders will be great. Event rates are being planned at the 100 MHz level, meaning that fast calorimeters must be built to minimize pileup. The experience at the Sp$\bar{p}$S of the importance of nearly full event containment (i.e. hermeticity) will be repeated. Many searches for new particles will demand good reconstruction of missing energy, for example the search for additional intermediate bosons such as $W' \rightarrow e\nu$. Excellent energy resolutions with good linearity and Gaussian resolution functions are required for many experiments, such as the search for compositeness at the tens of TeV energy scale.[19] The search for such structure in the high-p_T jet signature will test the best calorimeters. While all these performance characteristics are necessary, they must exist in a very hostile radiation environment.[20] Neutron fluxes in excess of 10^{12} cm^{-2} yr^{-1} and doses of greater than 10^3 Grays/year in calorimeters situated at a radius of two meters from the interaction point are anticipated at the next generation of hadron colliders. These requirements of performance and survivability will test the present understanding of calorimeter physics and designers' ingenuity in building radiation hardened equipment. The understanding of all fundamental processes is essential to a successful program.

The option of employing silicon detector diodes as the sampling medium in hadron calorimeters has been suggested in a number of previous works.[21,22] Successful devices have been constructed and tested using silicon diodes in electromagnetic calorimeters.[23] The advantages of extending this success to hadron calorimetry are numerous.[24] As an ionization sampling calorimeter, a silicon readout calorimeter would be a system of absolute gain. Silicon is a nearly nonsaturating medium so that sources can be used to get an absolute calibration of an energy scale. These devices can be operated at room temperature, eliminating the need for bulky and space wasteful cryostats required for other options. The signals have been shown to be relatively insensitive to magnetic fields. In principle the calorimeters can be made very compact due to the very thin sampling gaps required; since silicon diodes produce an electron-hole pair for every 3.7 eV deposited at room temperature, they require a much smaller sampling gap than most other systems. The technology of silicon diode fabrication makes fine lateral and longitudinal segmentation of silicon calorimeters easy and feasible. Finally, the property that provides the most promising feature of silicon diode readout is the speed of response. The intrinsic speed of normal diodes of thicknesses of 300 μm or so, is about 20 nanoseconds. Therefore, the speed of the front-end electronics is likely to limit the speed of response. However, achieving the optimal physics results at the future high rate colliders may well require calorimeters which exploit this intrinsic speed as fully as possible. It is for many of these reasons that the SICAPO Collaboration is working on the development of silicon hadron calorimeters.[25]

2. FUNDAMENTAL PHYSICS OF COMPENSATING CALORIMETERS

2.1 BASIC IDEAS

Before one is able to assess the prospects for hadron calorimetry with silicon, it is essential to understand the details of compensating calorimetry. This begins with an appreciation for the original motivation of the inventors of the technique.[26] It must be realized that hadronic cascades which contain large amounts of electromagnetic energy have less losses of energy due to nuclear break-up than those which contain little electromagnetic energy and therefore a large number of hadronic interactions. This comparison is illustrated in Fig. 1. Figure 1a shows the situation for noncompensating calorimeters. The overall distribution is created by summing a variety of different types of events. The two extremes, here called type A and type B, result in quite different responses. The type A events have a large fraction of the incident hadron energy converted to π^0 and other forms of electromagnetic energy, and therefore there are few hadronic nuclear interactions. Since the π^0 yield an observed signal which is comparable to the response of the calorimeter to incident electrons of the same energy and there is little energy lost to the breakup of nuclei, the e/h ratio for such events is nearly one, as shown in Fig. 1a. Type B events in such noncompensating calorimeters, on the other hand, show large amounts of lost energy in the nuclear break up resulting from the many hadronic nuclear interactions. This includes nuclear binding energy losses, as well as losses from heavy fragment production, neutrino production, and low energy nucleon generation. All of these processes result in a reduction in the detectable energy in the calorimeter. These type B cascades have a minimal amount of generated electromagnetic energy and the resulting e/h ratio is much less than one. Combining all types of hadronic cascades, from type A to type B and everything in between, leads to a very broad distribution of responses, and a resulting poor resolution for the measured energy deposition.

Figure 1b illustrates the situation for compensating calorimeters where the response to events of type A and type B have been equalized by a cleverly designed calorimeter. This is the basis for the original ideas as presented in Ref. 26. It can be seen from the figure that type A events respond with a signal nearly equal to an electron signal. However, the type B events also give an average response that is nearly comparable to the response of an electron. The nuclear breakup energy has been *compensated for*, by designing the calorimeter to preferentially respond to the low energy neutron component of the shower, which is correlated with the lost nuclear breakup energy. As will be shown later, it is not necessary to fully recover all of the nuclear breakup energy as the electromagnetic response is also suppressed in high Z materials due to processes occurring at the very low energy portion of the electromagetic shower. The role of these sampling inefficiencies which result from the preferential photon absorption[11] and the electron multiple scattering in the inactive material[6,9] has a very stong effect on the calorimeter response. A proper balance of the electromagnetic suppression and the preferential sampling of low energy neutrons leads to this equalization of the average response of type A and type B events. As a result, the sum of all the types of events, from A to B, yields a

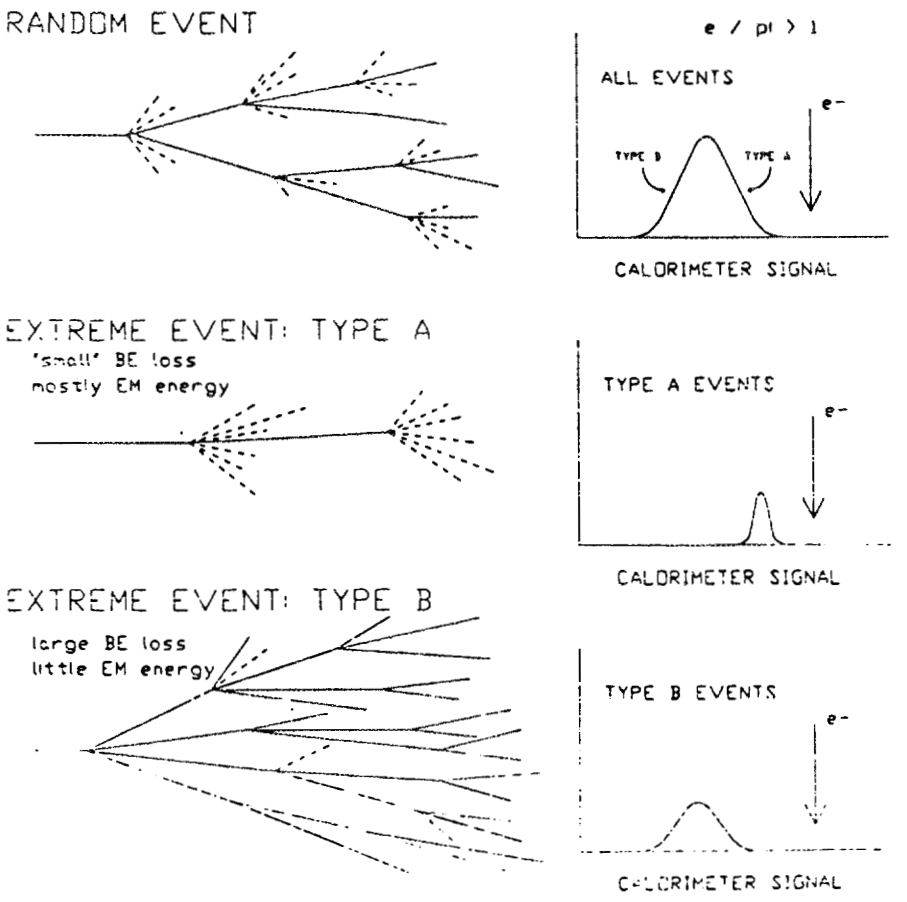

Fig. (1a). An illustration of the origin of e/h > 1 in noncompensating calorimeters.

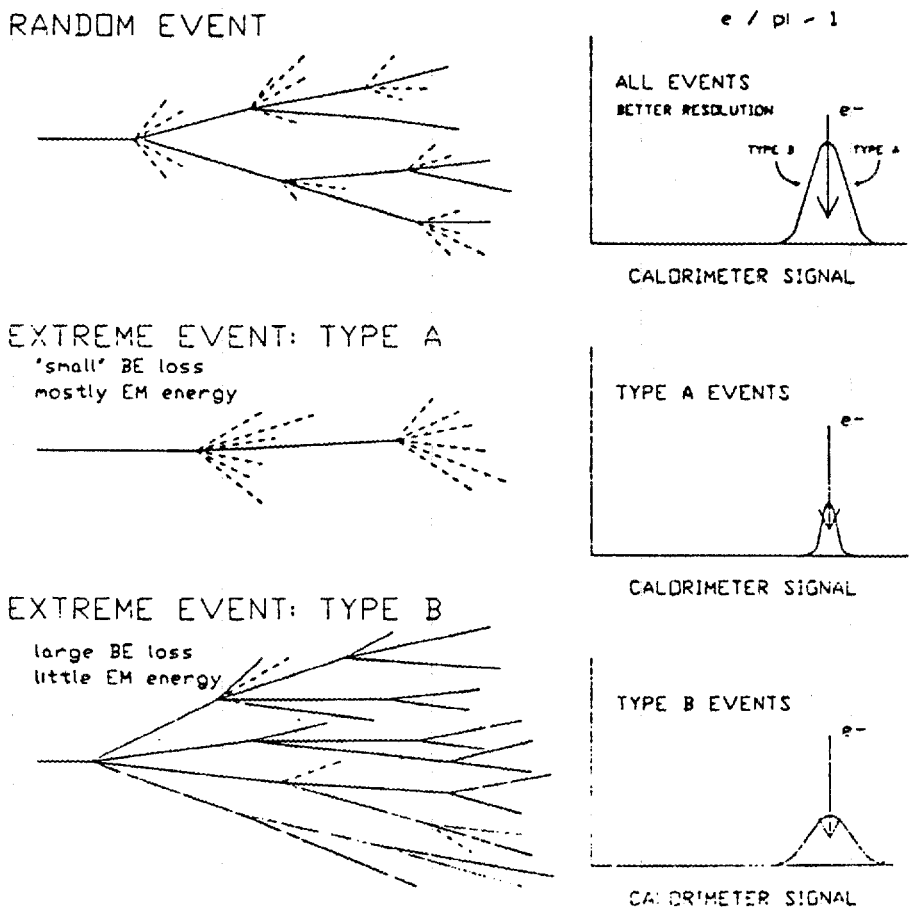

Fig. (1b). An illustration of the origin of e/h $\approx$ 1 in compensating calorimeters. This underlying role of electromagnetic and binding energy losses to the fluctuations in energy distributions was described in Ref. 26 to motivate the development of compensating calorimeters.

narrower distribution; that is, the energy resolution is greatly improved. This is the motivation for examining the ratio e/h as a measure of the degree of compensation.

2.2 BINDING ENERGY LOSSES

In previous studies of the detailed processes occurring in hadronic cascades, extensive use has been made of the CALOR code system (HETC, EGS, MORSE, MICAP, SPECT, LIGHT, etc.- see the Appendix for details).[27] Figure 2, for example, presents the calculated distribution from HETC of energy lost through the release of nuclear binding at the first interaction of a 5 GeV π^- in a uranium scintillator sampling calorimeter composed of alternating three millimeter uranium plates and scintillator sheets. An average energy loss of 380 MeV occurs at the first interaction sites. This represents 7.6% of the incident hadron's energy removed from the cascade at the first interaction. For lower energy interactions the loss is naturally going to be smaller, but only somewhat since for the same calorimeter HETC predicts an average loss of 200 MeV at the first interaction of 1 GeV incident neutrons. Notice that this represents twenty percent of the incident hadron kinetic energy. For lighter target materials, such as iron, the value will be somewhat less.[28]

As the shower progresses many additional interactions lead to an accumulated energy loss. Figure 3 shows the distribution of the number of nuclear interactions (excluding elastic collisions) in HETC for the incident 5 GeV π^- on this uranium scintillator stack. There are an average of 24 collisions,[29] while some showers terminate as the pion decays in the stack (note three of these 500 showers had no nuclear collisions). Integrating the binding energy loss over these many interactions yields the distribution of binding energy lost for the entire showers as shown in Fig. 4. On average 32% of the incident kinetic energy is lost in binding energy associated with the ejection of nucleons (primarily low energy) from the nuclei. A total of 1600 MeV has been lost in the form of binding energy, but one remaining effect is the large number of low energy neutrons created in the nuclear disruption. Figure 5 shows the correlation of the energy content of the low energy spallation and evaporation neutrons (kinetic energy below 20 MeV) with the binding energy lost in each of the hadronic cascades. Events with small binding energy losses naturally have disrupted the nuclei to the smallest extent and have transferred the least energy to low energy nucleons. Events with large binding energy losses have resulted from a large number of very disruptive collisions, resulting in large amounts of energy being carried by the low energy nucleons. These trends are very evident in Figure 5. It was this strong correlation which motivated the first attempts at the construction of compensating calorimeters.[26] It was reasoned that by increasing the neutron content through the fission process in the calorimeter, the binding energy losses could be overcome in a fashion which was proportional to the losses, thereby leading to an improved resolution. To achieve this end, uranium was employed as a radiator material.

2.3 NEUTRONS

The key to successfully capitalizing on this correlation is through the coupling of these low energy neutrons to the sampling medium. Eventually, most of these low energy neutrons are captured by ^{238}U, yielding approximately eight MeV per neutron capture in prompt gammas. In addition, prompt fission gammas are

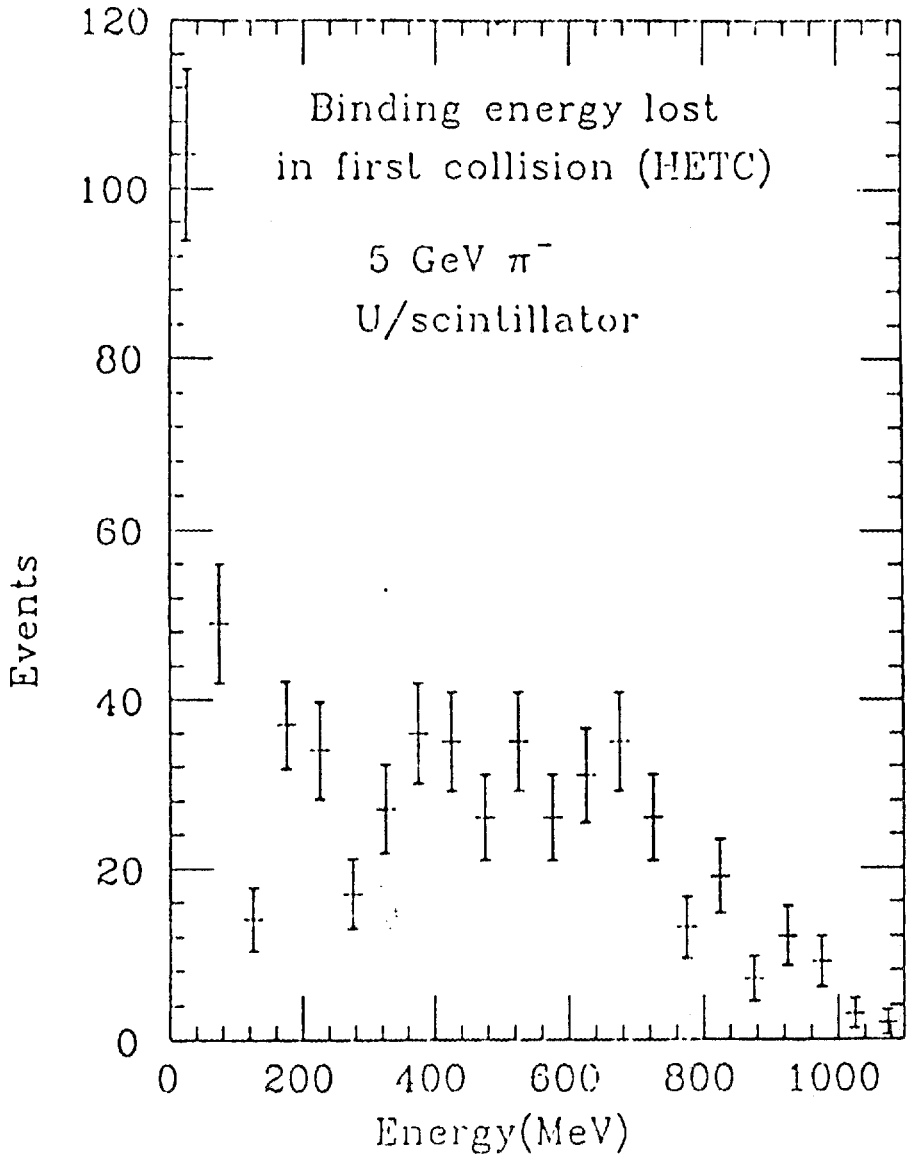

Fig. 2. The distribution of binding energy lost in the first collision of a 5 GeV π^- on a uranium-scintillator calorimeter made of 3 mm uranium plates and 3 mm scintillators sheets as calculated by HETC. The average value is 380 MeV.

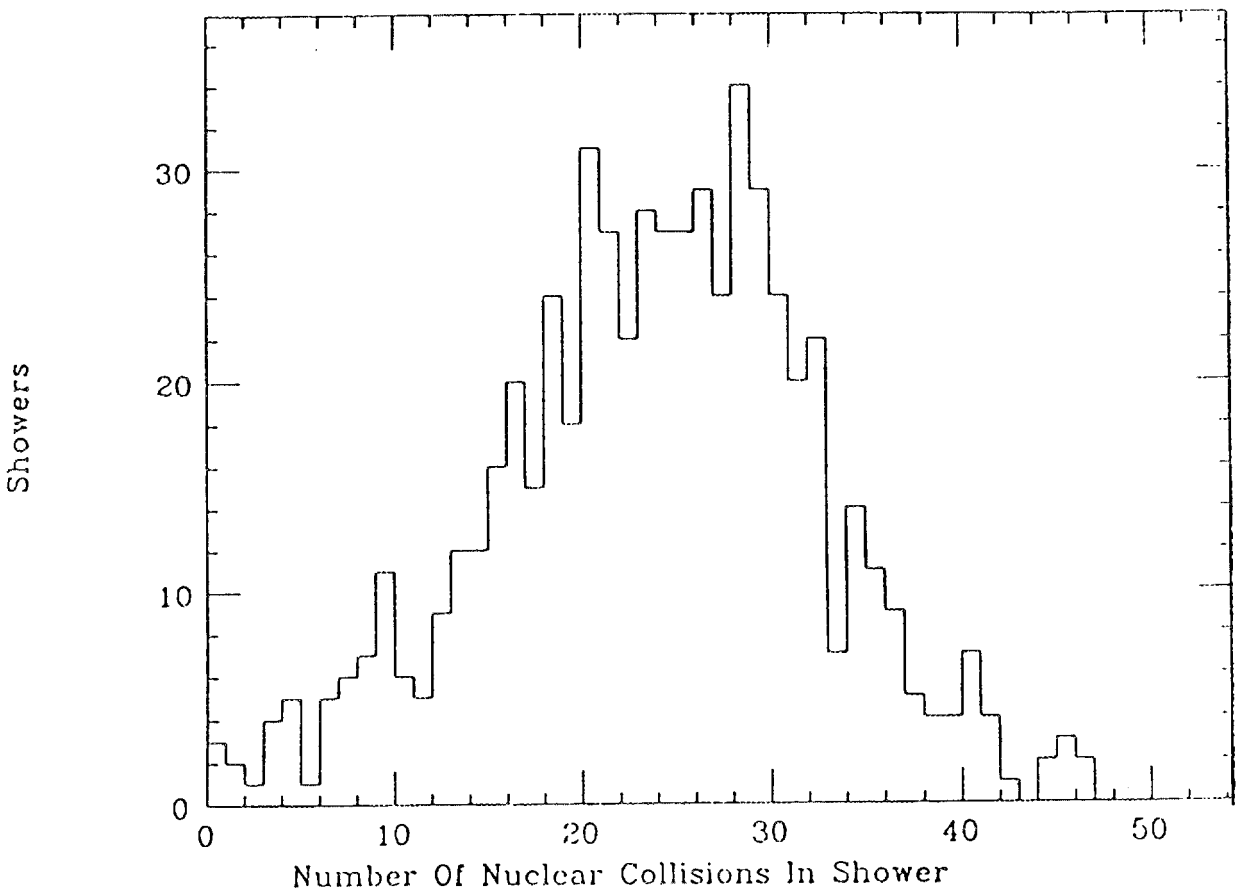

Fig. 3. The distribution of the number of nuclear interactions by a 5 GeV π^- on a uranium-scintillator calorimeter made of 3 mm uranium plates and 3 mm scintillator sheets as calculated by HETC. The neutrons in the cascade are cut off for this count at 20 MeV. The average number of collisions is 24.

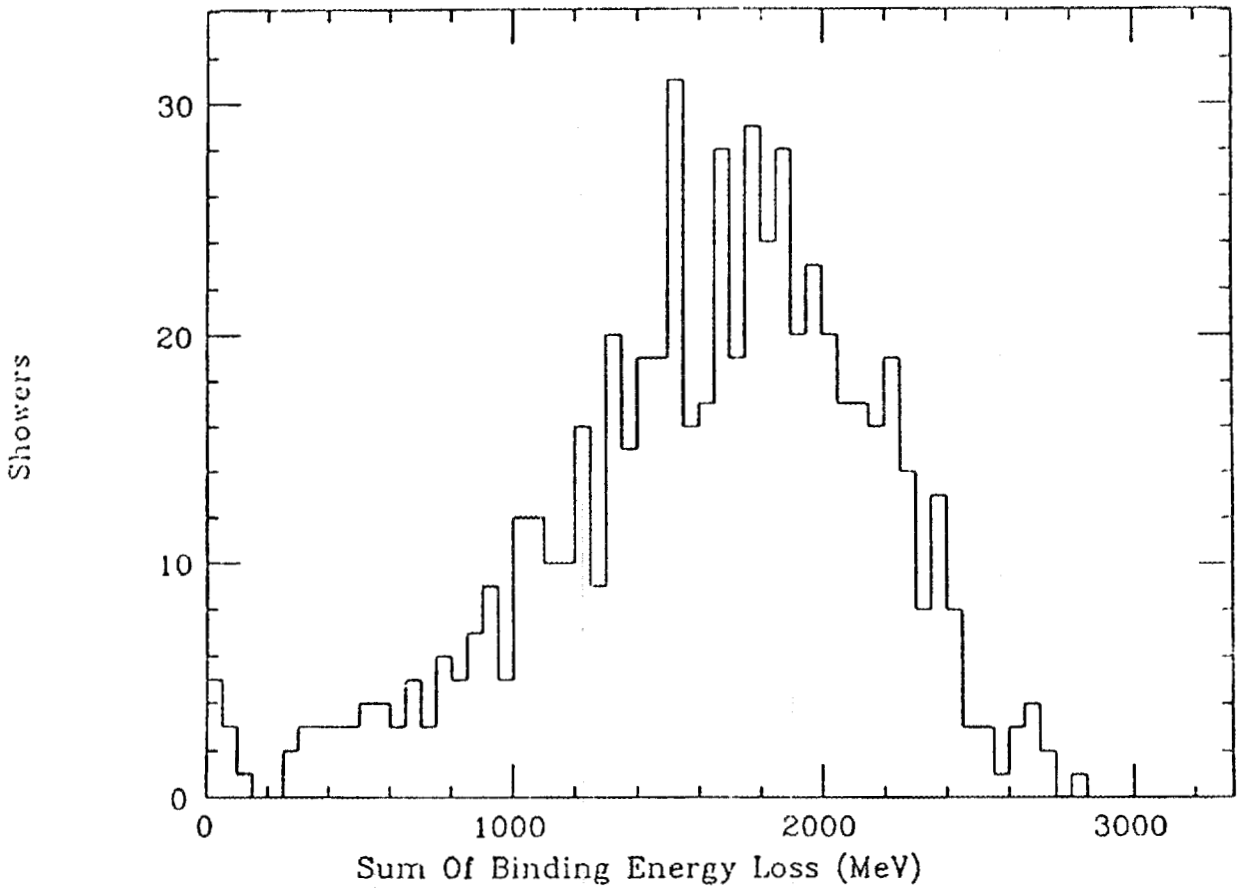

Fig. 4. The distribution of totla binding energy losses per shower from a 5 GeV π^- on a uranium-scintillator calorimeter made of 3 mm uranium plates and 3 mm scintillator sheets as calculated by HETC. The average energy loss is 1600 Mev, 32% of the incident particle energy.

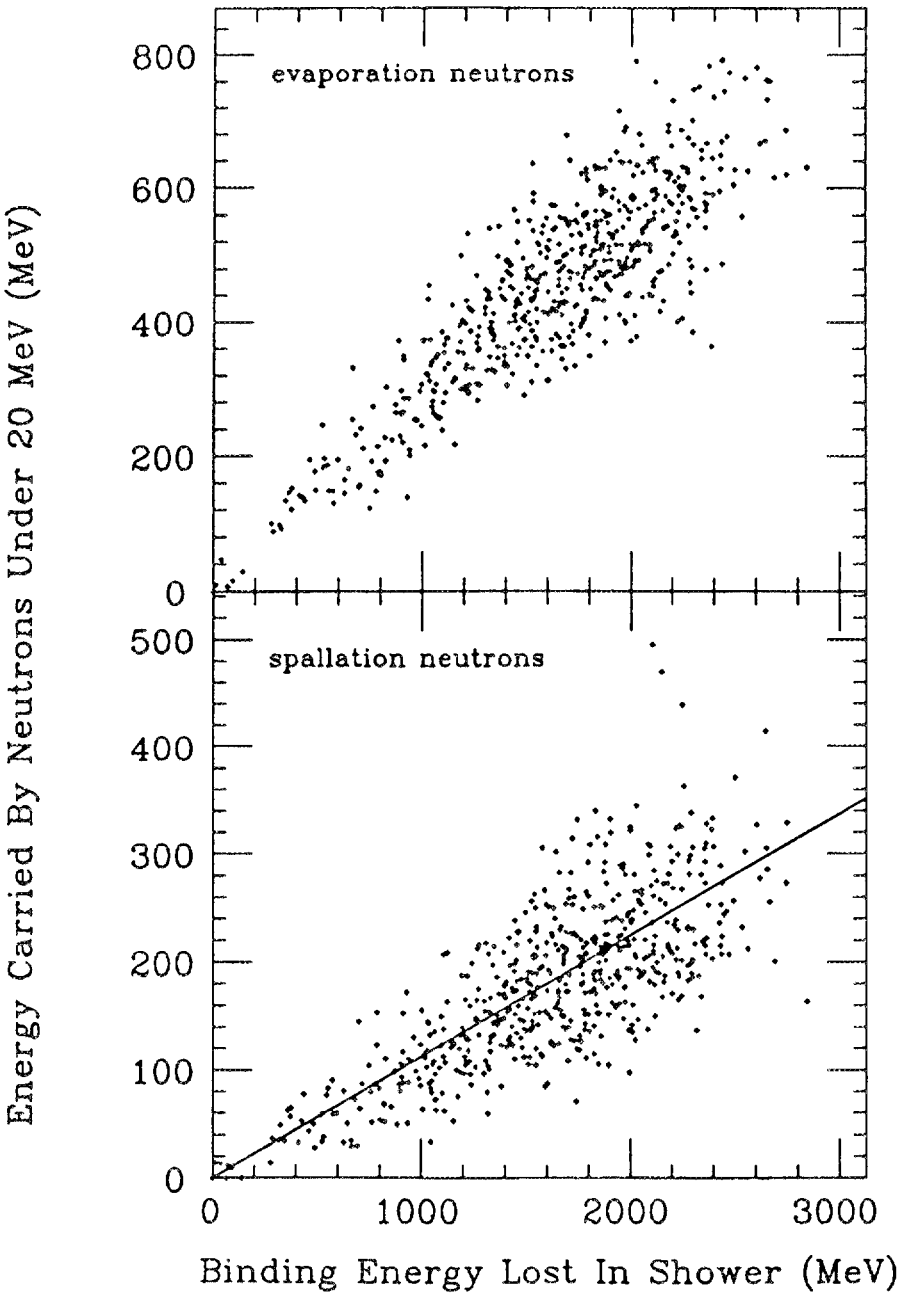

Fig. 5. The correlation of energy carried by neutrons below 20 MeV to the binding energy lost in showers from 5 GeV π^- on a uranium-scintillators calorimeter made of 3 mm uranium plates and 3 mm scintillator sheets as calculated by HETC. The distribution is presented both for the evaporation neutrons and the spallation neutrons. The solid line shows the average trend of the data and is plotted for comparison with Fig. 6.

produced in the fission process. Unfortunately, the sampling medium is very inefficient to sampling these soft gammas due to the effects mentioned earlier regarding preferential absorption in the high Z material. Also the time scale associated with thermalization of the neutrons is too long ($\sim$ μsec). Therefore, the signal from the neutrons must come from their direct interaction in the active medium.[30] Figure 6 shows the observed neutron energy which our calculations predict will be sampled by the plastic scintillator in the three millimeter uranium-scintillator stack. This distribution results from detailed calculations which were performed with the Oak Ridge Monte Carlo Codes HETC and MORSE (see the Appendix for details.) The solid line drawn on this figure represents the average energy carried by the spallation neutrons before transport; this is the same line as is shown on Fig. 5. Notice that a sizeable fraction of the original neutron energy (even after the effects of saturation have been taken into account) has been observed ($\sim$ 12%). This is due to neutron amplification by fission of the uranium and the very efficient transfer of neutron energy to the hydrogen, which will be discussed later. For comparison, the fraction of electromagnetic energy observed is about 6%.

Since the transfer is so complete in the hydrogenous plastic scintillator, the relative contribution of the total signal can be varied by changing the relative thickness of the sampling layer and the uranium radiator, as was pointed out first in Ref. 13. This is illustrated in our calculations shown in Fig. 7. A calorimeter composed of three millimeter uranium plates and 3 mm plastic scintillator plates gives approximately the correct fraction of neutron coupling to bring the e/h ratio to 1.0. When the radiator thickness is increased to 6 mm, the scintillator thickness must be considerably greater than 6 mm to achieve e/h = 1.0. The neutron energy has been significantly reduced by the first 3 mm of scintillator and therefore the doubling of thickness does not double the neutron coupled energy.

It is important to understand in detail the fission processes which take place in the calorimeter stack. Recent activation analysis measurements[16] have confirmed the basic level of fissions calculated with the CALOR code system.[31,32] Recently, calculations[33] were carried out to determine the numbers of fissions induced by neutrons of kinetic energies below 20 MeV for the two stacks studied experimentally as reported in Ref. 16. Reasonable agreement has been obtained for the massive uranium stack case (5.6 $\pm$ 0.3 /GeV calculated compared to the experimental 6.4 $\pm$ 0.7 /GeV), but the size of the measured number of fissions for the uranium-scintillator case remains a puzzle (2.4 $\pm$ 0.2 /GeV calculated compared to the experimental 5.1 $\pm$ 0.7 /GeV.) One would expect the number to drop by a larger fraction than measured as the coupling of the neutrons to the hydrogen in the plastic scintillator rapidly drops the neutron energies below the fast fission threshold of ^{238}U at approximately 1 MeV.

Accurate predictions of performance also require a knowledge of the relative time of response for the various components of the calorimeter signal. The temporal response functions for the fission and neutron capture processes expected in an infinite natural uranium system were presented in Ref. 31. Since the capture energy will be inefficiently transferred to the signal, the majority of the hadronic response of uranium calorimeters occurs in the first 50-100 nanoseconds.

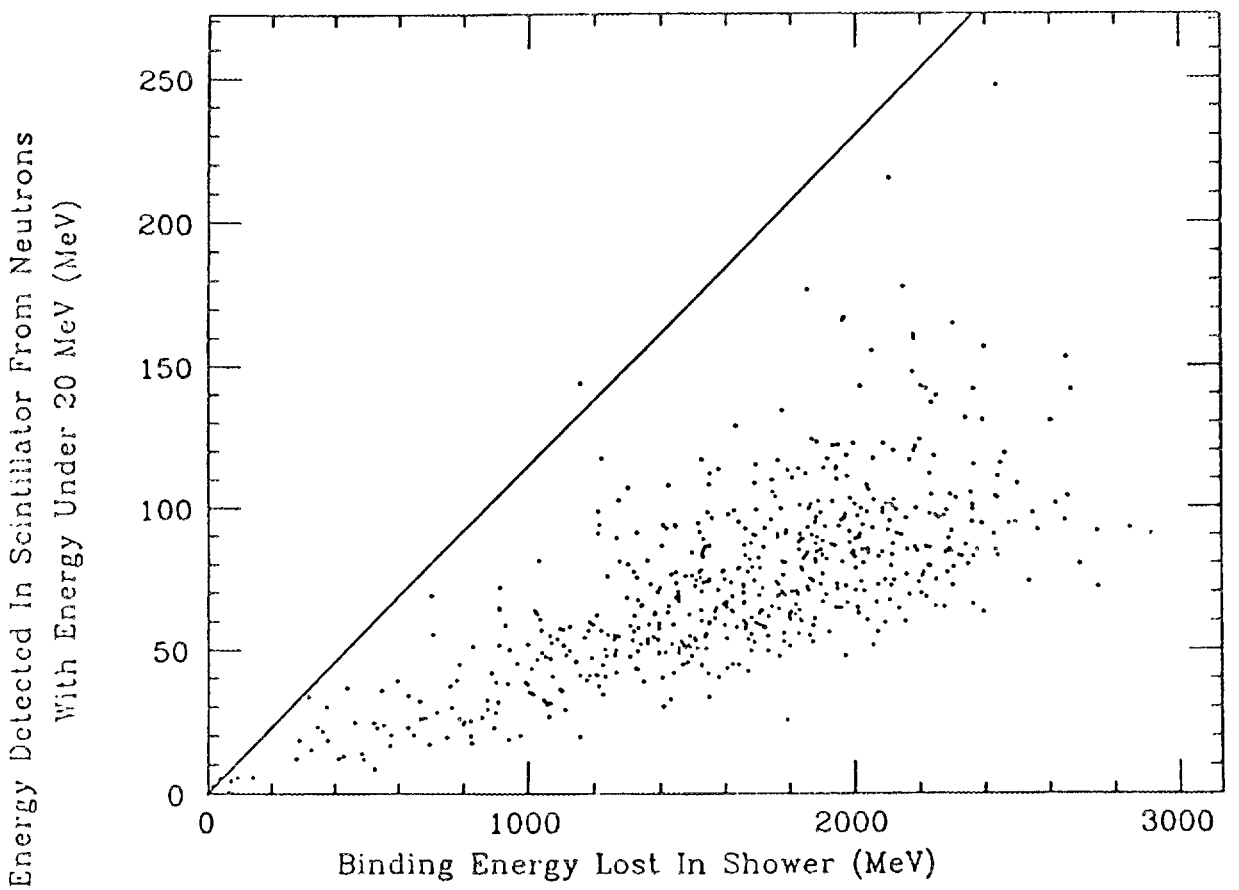

Fig. 6. Calculations of the energy detected in a 3 mm uranium/3 mm scintillator calorimeter stack from the neutrons with energy below 20 MeV versus the binding energy lost in showers from 5 GeV π^-. The solid line shows the average trend of the data in Fig. 5. See text for discussion.

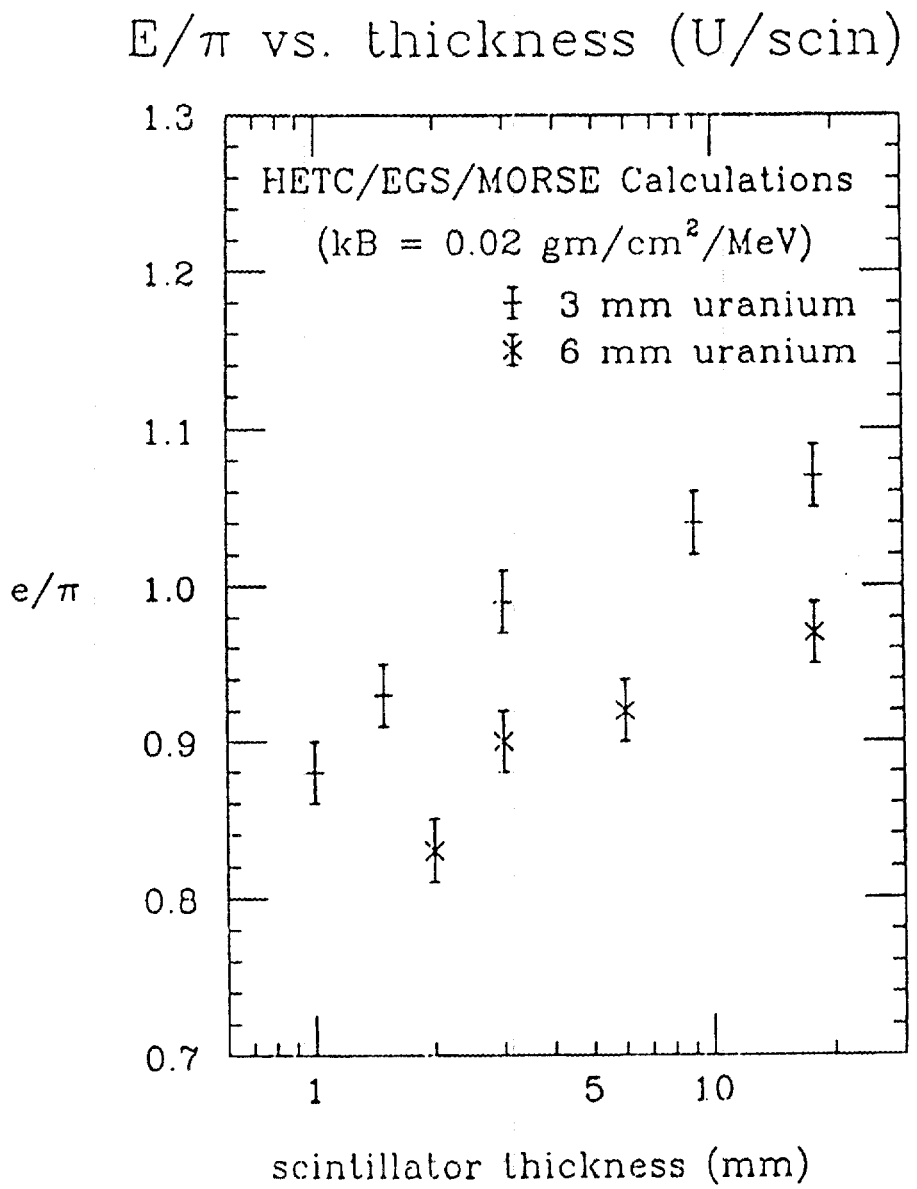

Fig. 7. The variation of e/π with scintillator thickness for a set of uranium-scintillator calorimeter calculations for incident 5 GeV π^-. This figure illustrates the "tuning" possible with scintillator, first noted in Ref. 13.

2.4 EARLY CALCULATIONS

All of the effects mentioned above were included in our earlier studies of compensating calorimeters. A review of these earlier calculations is useful to understand the new results to be presented later. Figure 8 shows comparisons between calculations[7] and AFS measurements[34] for various ratios of iron (copper) and uranium in the calorimeter. Note that for these comparisons, the differences between iron and copper do not alter the basic results and conclusions. As the data and calculations show, the compensation resulting from increasing fractions of uranium radiator is well understood.

In this same study, the response of a uranium-liquid argon calorimeter was found to be less compensating. The selection of events can alter the conclusion on the degree of compensation by reducing the e/h ratio and narrowing the energy distribution. References 7 and 8 pointed out this selection bias, and the importance of selection in the analysis was confirmed by the experimenters.[35]

2.5 HYDROGENOUS MEDIA

This very different response of uranium calorimeters employing different readout media was interpreted[7,8] to yield the new understanding of compensating calorimetry. The underlying phenomena responsible for the significant difference were explained in terms of three basic differences of the sampling materials.[8] First, the neutron cross sections in hydrogen continue to rise below 1 MeV, while the cross sections in argon are falling (see Fig. 9. This in itself means that a larger fraction of the soft neutron energy will be deposited in the plastic scintillator than in the liquid argon. Secondly, the kinematic constraint on the energy transferred in a neutron-nucleus collision highly favors the transfer of energy to a lighter nucleus. The maximum possible recoil energy ($E_R|_{max}$) transferred from an incoming nonrelativistic neutron of kinetic energy E_n to a recoil nucleus of atomic weight A can be shown[36] simply from conservation of momentum and energy to be

$$E_R|_{max} = \frac{4A}{(1+A)^2}\ E_n. \tag{1}$$

This means that in neutron-hydrogen collisions, the full energy of the neutron can be transferred, while in neutron-argon collisions the maximum energy which can be transferred is ten percent of the neutron energy. Thirdly, the energy coupling is even more suppressed in liquid argon due to the saturation which occurs in regions of dense energy loss. In scintillators this phenomenon has been studied for many years and was modeled by Birks[37] in a form that has come to be known as Birks' Law:

$$\frac{dL}{dx} = \frac{S\frac{dE}{dx}}{1 + kB\frac{dE}{dx}}, \tag{2}$$

where $\frac{dL}{dx}$ is the light yield per unit path length, $\frac{dE}{dx}$ is the specific energy loss for the charged particle, S is the normal scintillation efficiency, and the kB parameter describes the quenching which occurs for high density ionization. Typical kB factors for scintillators are 0.01-0.02 gm cm^{-2} MeV^{-1}. Following the suggestion of Ref. 7, it has become customary to express the columnar recombination[38], which results

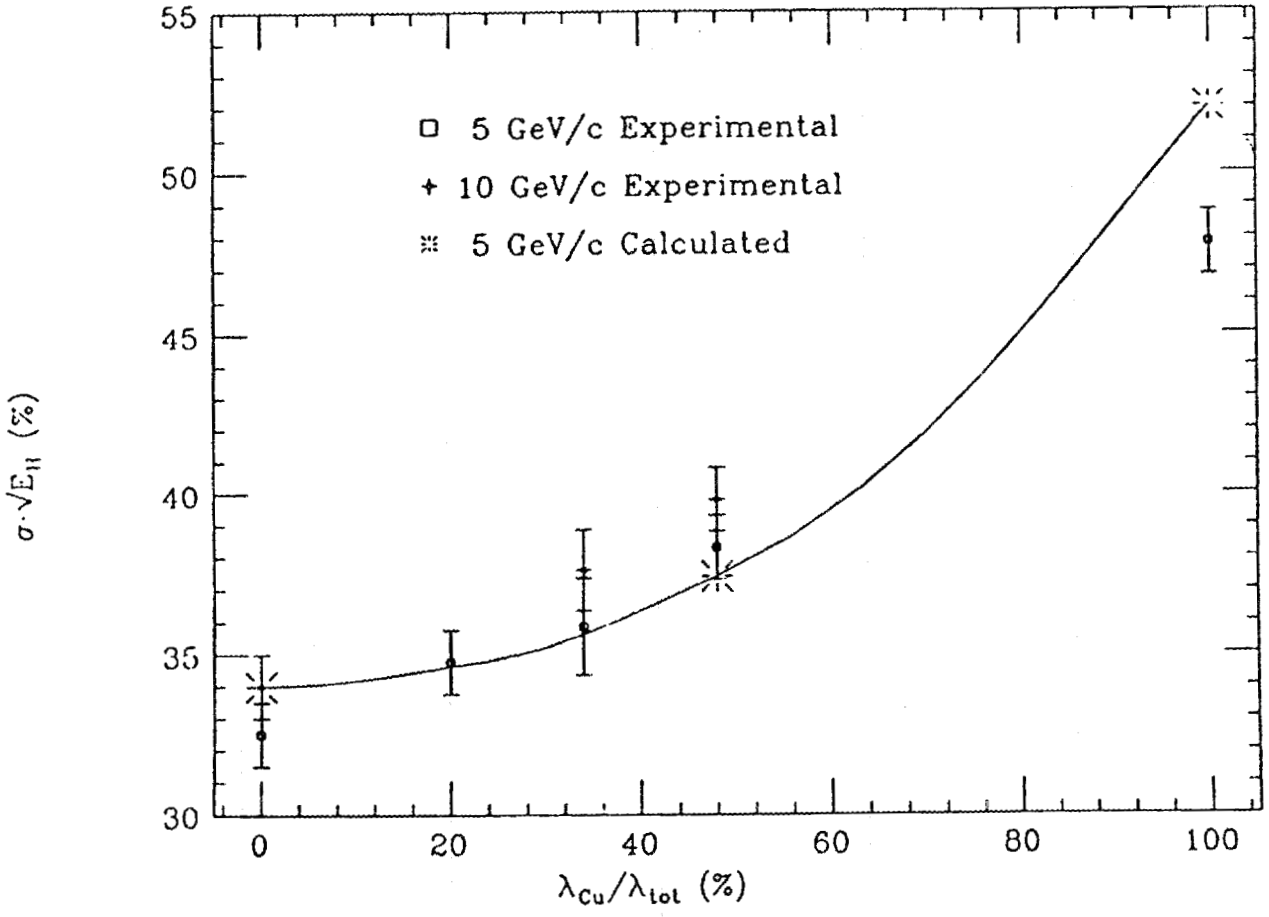

Fig. 8. The comparison of the simulation[7] of the dependence of hadron energy resolution with uranium purity with the experimental measurements of the AFS Collaboration.[34].

in saturation in liquid argon ionization sampling calorimeters, also in the form of the Birks' Law. In this form the equivalent kB factor for liquid argon is about 0.005 gm $cm^{-2}MeV^{-1}$, which is less saturating than scintillator. While the intrinsic saturation in liquid argon is less than in scintillator, the kinematic constraint on the energy transfers in neutron-nucleus collisions leads to a greater suppression of the transfer of neutron energy to observable signal. In liquid argon the highly ionizing recoil nuclei receive only one-tenth the relative energy of the less highly ionizing recoil protons in scintillator.

Qualitatively it is easy to see why the saturation has so much more of an effect by examining the calculations of Refs. 7 and 8. The 5 GeV protons studied in those calculations were found to deposit 402 MeV into the liquid argon gaps of 2.0 millimeters (the uranium thicknesses were 1.7 mm). However, due to saturation, only 308 MeV was detectable. The effect of this was to raise the e/h ratio to 1.2 from a potential value of 0.9 in the absence of saturation.[39] Of the 94 MeV lost to saturation, 72 MeV comes from collisions of the low energy ($<$ 20 MeV) neutrons. Therefore, the saturation of the energy delivered to the liquid argon has reduced the degree of compensation from an over-compensation condition to a value of 1.2. Note that this calorimeter was restricted in transverse dimension, particularly the uranium portion, and therefore a larger device would be expected to obtain smaller values of e/h. Furthermore, these calculations of e/h were subsequently confirmed by the experimenters.[35]

2.6 ELECTROMAGNETIC SAMPLING

It is important to recognize the significant effects of reduced electromagnetic response in calorimeters composed of high Z radiator structures.[11] These "electromagnetic sampling inefficiencies" have been explained as resulting from the preferential absorption of low energy photons ($<$ 1 MeV) in the high Z material and the effective electron path length stretching in the inactive media resulting from enhanced multiple scattering in the high Z material.[6,9,13] Figure 10 displays how the preferential absorption of the low energy photons in the high Z material occurs. Here the photon mass attenuation coefficient multiplied by the fraction of primary photon energy loss for argon and for lead can be seen.[40] Clearly, in the high Z material, the relative absorption at low energy, say $\sim$ 100 keV, is much more effective in stopping the photons. The role of multiple scattering has also been clearly demonstrated by examining the effect of turning off multiple scattering in the electron-gamma shower program EGS.[41] Such calculations for 1 GeV electron showers in uranium liquid argon sampling calorimeters show an increase of 10% in the signal deposited in the liquid argon as the electron path length stretching disappears.[6,9] The magnitude of this "electromagnetic sampling inefficiency" is often measured by comparing the response of a calorimeter for incident electrons to that anticipated for minimum ionizing particles. The ficticious fully contained minimum ionizing particles can be measured by scaling up the response of the calorimeter to muons. Such measurements find the ratio of average electron pulse height to the pulse height for the minimum ionizing particle to be roughly 0.6 to 0.7 for calorimeters constructed with high Z radiators. The magnitude of this effect led us to the prediction "that a lead calorimeter may also give EM/HAD $\approx$ 1."[13] This prediction has now become reality. A lead-scintillator compensating

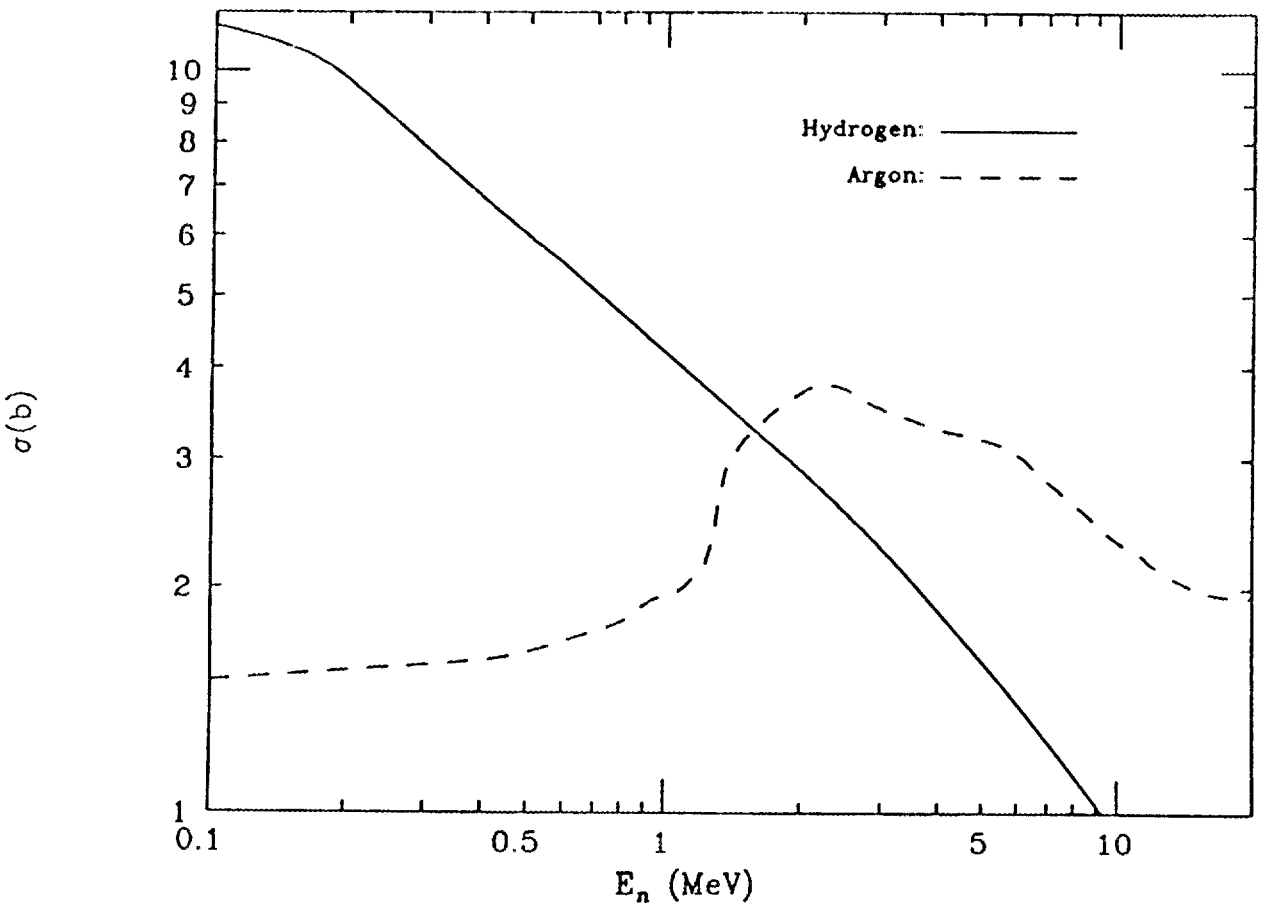

Fig. 9. Comparison of the neutron total cross sections in hydrogen and argon. The argon cross section represents the average value in the regions of much structure. (These are approximate curves presented only for comparison.)

calorimeter has been built and tested with scintillator thicknesses of one-fourth the lead thicknesses, a ratio designed to give the optimal electron to hadron ratio.[15] The reported e/h ratio for this device is 1.05 ± 0.04 for energies over 10 GeV. Caution should be exercised, however, since this analysis is based on events selected by energy deposition. This selection could emphasize the electromagnetic parts of the hadronic shower and yield a biased e/h ratio.

The understanding of the underlying phenomenology of compensating calorimeters is on solid ground and calculations can be done reliably. The requirements of the future hadron colliders demand that wise use be made of this understanding.

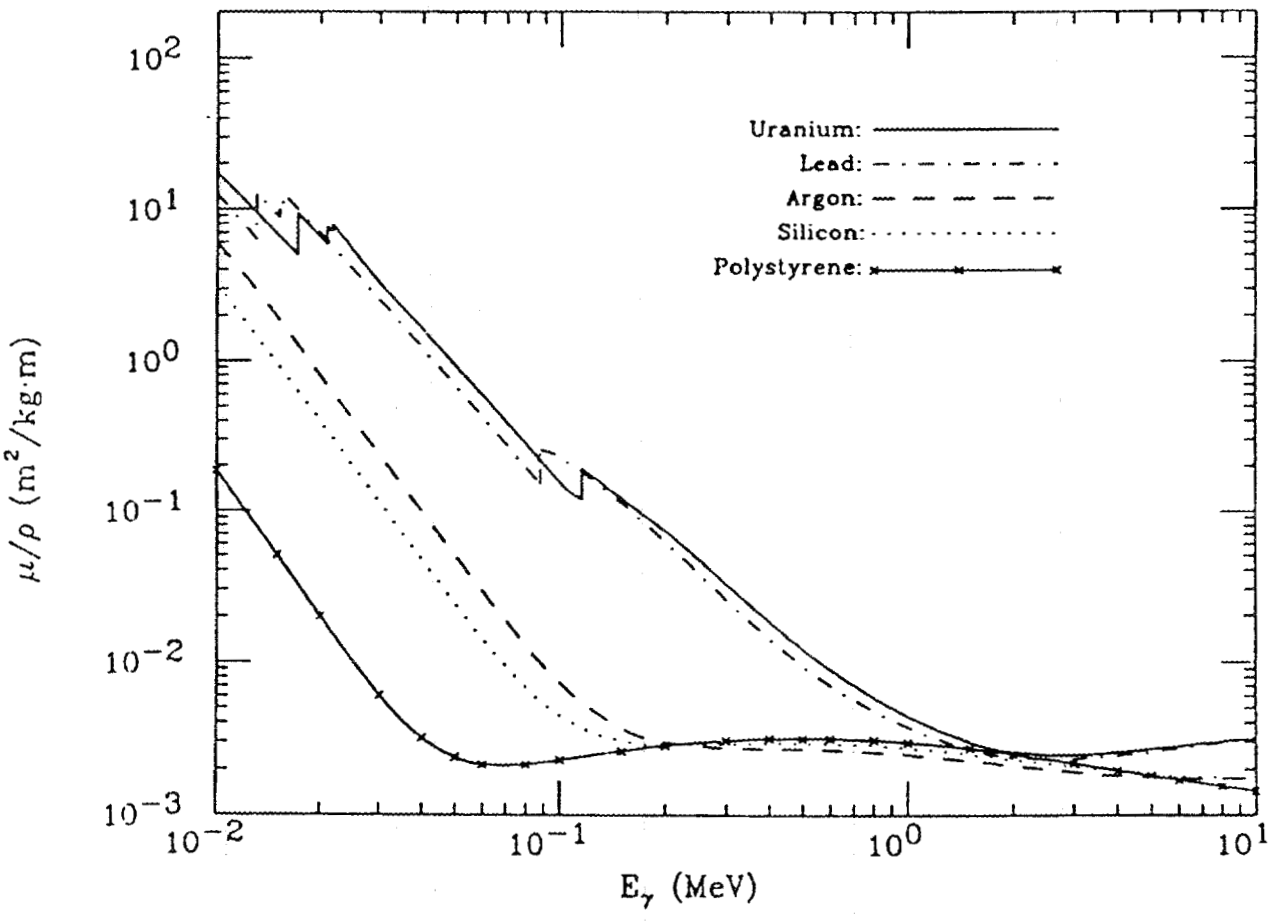

Fig. 10. Comparison of the photon mass attenuation coefficients multiplied by the fraction of primary photon energy loss for polystyrene, silicon, argon, lead, and uranium.

3. CALCULATIONS OF SILICON HADRON CALORIMETERS

The understanding that now exists concerning compensating calorimeters can be applied to the silicon detector calorimeters. The fundamental question that needs to be addressed is what the e/h ratio for these silicon based calorimeters will be. One property of silicon that plays an important role in this study is the extreme linearity of silicon up to very large stopping power.[42] That is, silicon exhibits very little saturation. It has been demonstrated that saturation prevents full compensation in currently designed uranium-liquid argon calorimeters, so this could be a very important factor in silicon calorimeters. Naively, it is expected that very good results can be obtained for silicon calorimeters.

The linearity of response of silicon to large energy deposition densities is summarized in Fig. 11. This figure shows the relative response of a recoil ion of maximal energy in neutron scattering.[43] One sees that even for silicon ions as low as 100 keV nearly one-half of the deposited energy is detected as observable output signal. Given these evidences of very limited saturation in silicon detectors a very good response to some components of the low energy development of hadronic showers can be expected.

It is pedagogically useful to consider the differences between the response of silicon and liquid argon, since except for the saturation in liquid argon, full compensation could possibly be achieved. The three critical factors which were reviewed earlier to compare the neutron coupling to scintillator and liquid argon are useful to compare again here. First, the neutron cross sections[44] are compared in Fig. 12. It can be seen that the cross section in argon falls for energies below a few MeV, while the cross section in silicon remains large and even rises below 500 keV. This will result in a larger energy depostion by low energy neutrons in silicon than is observed in liquid argon. The typical neutron energy spectrum which has been calculated in these studies[33] is also shown in this figure and illustrates the importance of the cross sections at the lowest energies. Secondly, the effect of the kinematic limitation on neutron energy transfer can be considered. Equation 1 shows that while only one-tenth of the neutron energy can be transferred in liquid argon collisions, the restriction on energy transfer is somewhat less restricted in silicon, being limited to about 13 percent. This should lead to an additional increase in the energy transferred to the silicon. Finally, the very limited saturation which occurs in silicon will enable these increased neutron depositions to be more observable.

The potential for compensation with silicon certainly seems better than for liquid argon. To make quantitative predictions it is necessary to make use of a Monte Carlo code[27] system which takes into account all of the basic processes and examines the details of the shower development. As in our earlier studies, the Oak Ridge system CALOR has been applied to this problem. The details of this system are described in the Appendix. It has been assumed that the effective kB parameter in Birks' law is equal to 0, an approximation which should be very good for these studies. The e/h ratio will be only slightly underestimated in these calculations.

Figure 13 shows the calculated response distribution for 10 GeV π^- incident on a silicon calorimeter with 5 mm thick uranium radiators and 400 μm fully depleted

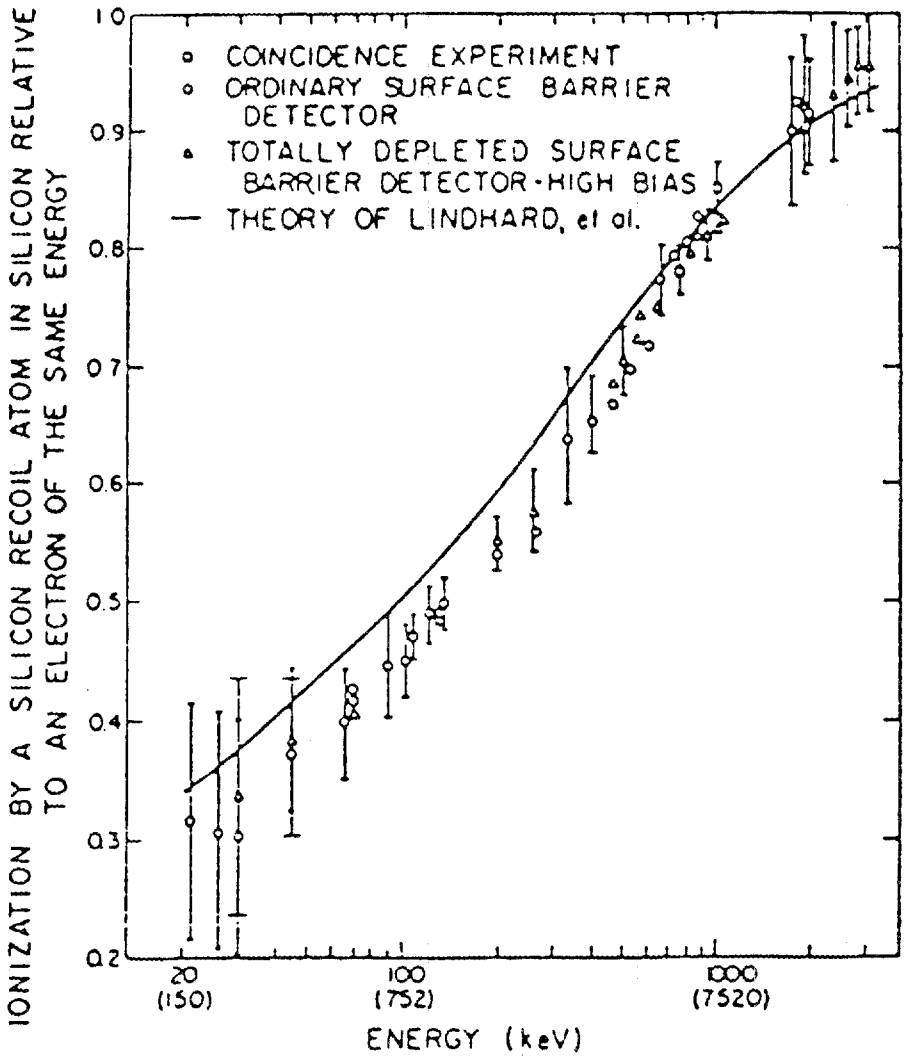

Fig. 11. Pulse height produced by a Si recoil atom relative to that of an electron of the same energy in Si as a function of Si recoil energy. The incident monoenergetic neutron energy necessary to produce the denoted recoil energy is shown in parenthesis. (From Ref. 43.)

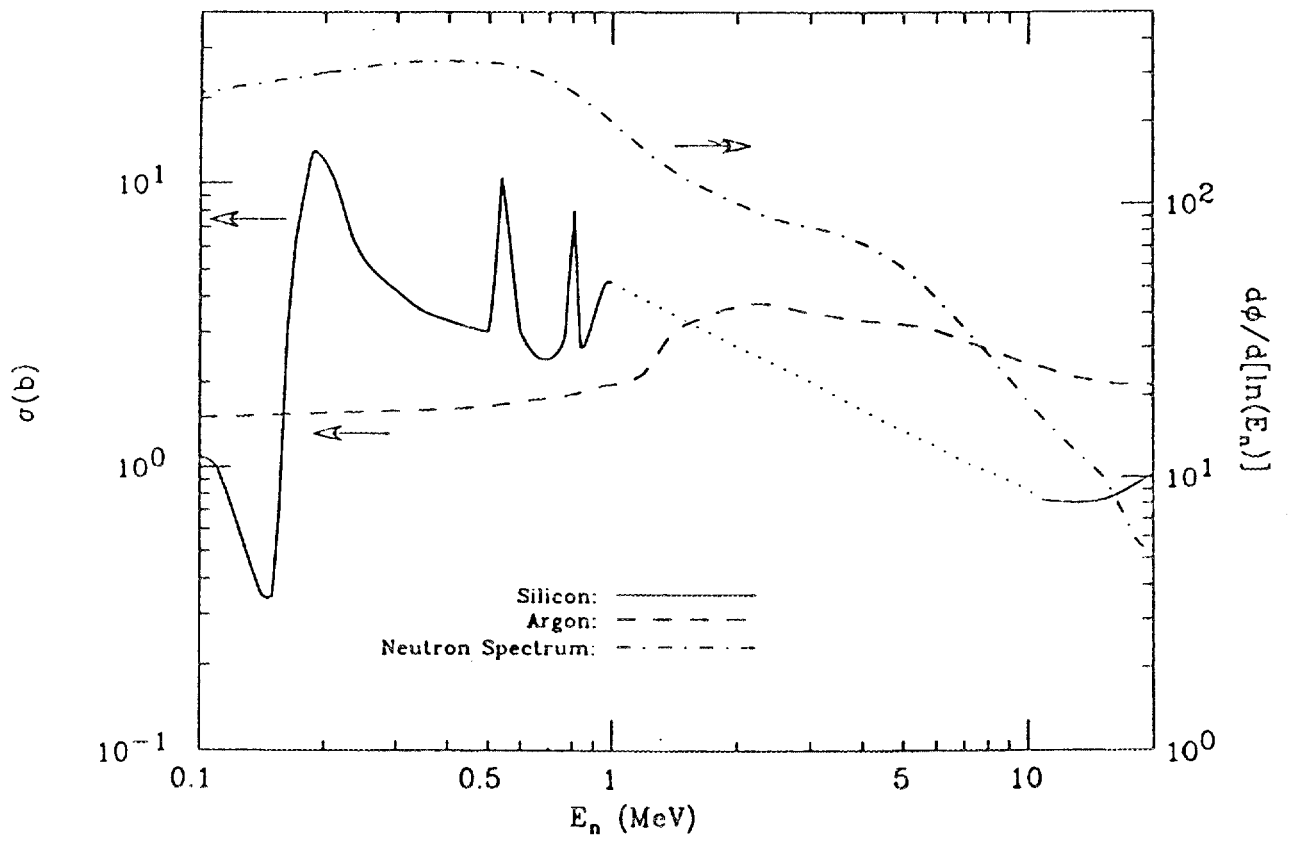

Fig. 12. Comparison of the neutron total cross sections in silicon and argon. The silicon and argon cross sections represent the average in regions of much structure. (These are approximate curves presented only for comparison.) Also shown on this figure is the typical calculated neutron energy spectrum from Ref. 33.

silicon detectors sandwich between two layers of 5 mm thick G10. Therefore, the total layer thickness is 15.4 mm and the depth of the stack extends for 150 readout and radiator layers. The transverse dimensions of the stack have been taken to be 100×100 cm^2. The charge collection is cut off after 50 nanoseconds. The resulting energy resolution (σ/E) is 21.5% and the e/h ratio is 1.07, close to compensation.[45] In fact, the two layers of G10 in this stack are increasing the value of e/h as the neutron energy from the uranium is being deposited in the G10 through the large energy transfers via hydrogen. Additionally, significant transfers occur to the carbon and oxygen in the G10.

Figure 14 presents the event by event correlation of the energy detected in the silicon from the low energy (<20 MeV) neutrons to the binding energy lost in the hadronic cascade. While the correlation is strong, this figure shows much larger fluctuations in detected energy than was seen in Fig. 6 for the uranium-scintillator calorimeter. This fluctuation depends on the number of neutrons actually detected. Given the very thin detection layers, the number of neutrons actually detected is small. Unlike the normal shower fluctuations which vary as $\sqrt{t_{cell}}$ and are dominated by the thickness of the radiator, the fluctuation on neutron response is dominated by the thickness of the silicon (t_{Si}), and scales as $\sqrt{t_{Si}}$. Therefore, the sampling fluctuations for the charged hadrons in the hadron cascades will be similar to any other readout medium, but the additional larger fluctuations on the neutrons will add to the width of the energy distribution, preventing excellent low energy resolution even for perfectly compensating calorimeters.

Figure 15 presents a series of calculated results for calorimeters constructed with 2 mm uranium radiators, followed by a layer of G10 of varying thickness and a 400 μm fully depleted silicon detector. As before, $kB = 0$, the time cut is 50 nanoseconds, and the transverse size is taken to be 100×100 cm^2. The stacks contain 330 layers of uranium, G10, and silicon. It can be seen that with no G10 the condition of overcompensation is obtained due to the sensitivity of the silicon detectors to very low energy particles. As the G10 is added, the e/h ratio increases due to the removal of neutron energy by the G10, meaning less energy is available to be deposited in the silicon. Naively, one might expect that the neutrons interacting in the G10 would contribute to the response of the silicon by knocking protons into the detectors. It has been proposed[7] that coupling a hydrogenous material to liquid argon, for example, would be a possible method for restoring its potential for compensation. However, the efficiency and range of the protons produced in the G10 is not large enough to have much of an effect on the total response of a detector of 400 μm thickness.[46] It can also be seen in Fig. 15 that the energy resolution reaches a minimum at approximately the point where the e/h ratio passes through one, as would be expected for a compensating calorimeter. The value of this resolution is not as small as the values achieved in scintillator because of the larger sampling fluctuations involved here, as described previously.

Several cases of silicon calorimeters have also been studied with different radiator materials, specifically one employing lead and one employing iron. For a lead calorimeter with 3 mm thick radiators and 400 μm fully depleted silicon detector with no air gaps and the same transverse geometrical constraints and time cuts as before, the calculated results yielded an expected e/h ratio of 1.16 with an energy resolution of $\frac{\sigma}{\sqrt{E}} = 47\%$ for 10 GeV π^-. For an iron calorimeter with 7.5 mm

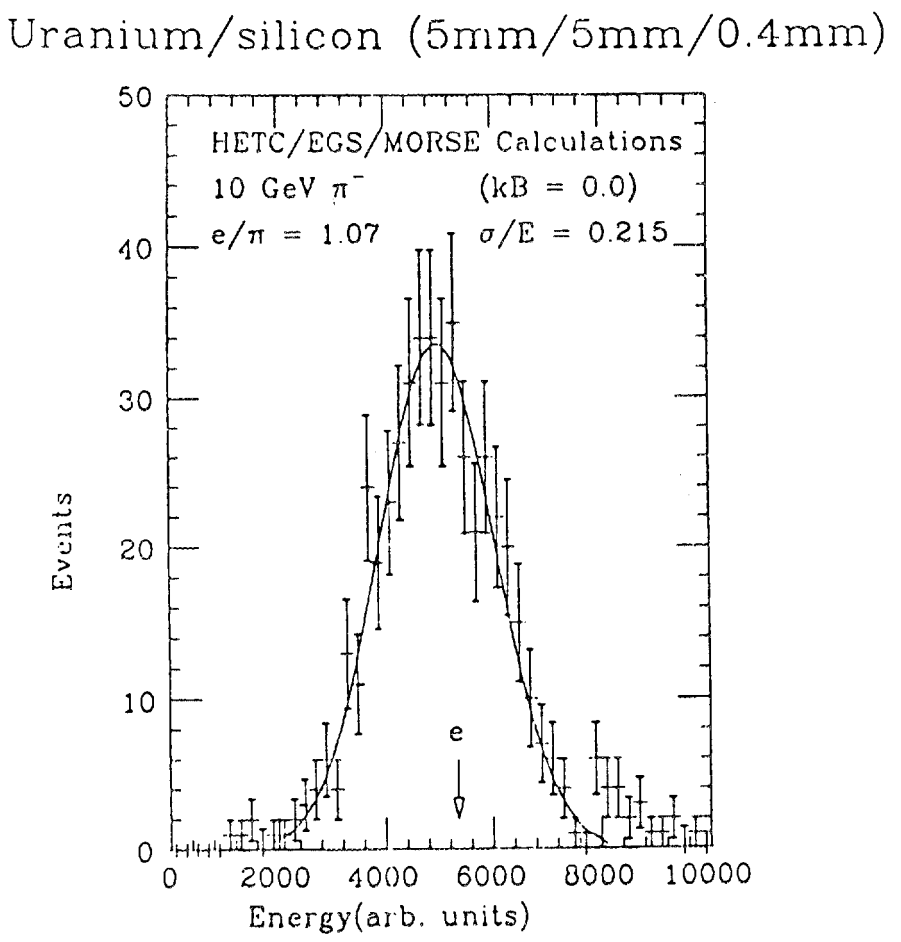

Fig. 13. The calculation of the measured hadron energy distribution for 10 GeV π^- incident on a uranium-silicon calorimeter with 5 mm thick uranium radiators and 400 μm fully depleted detectors imbedded in 5 mm thick G10 supports.

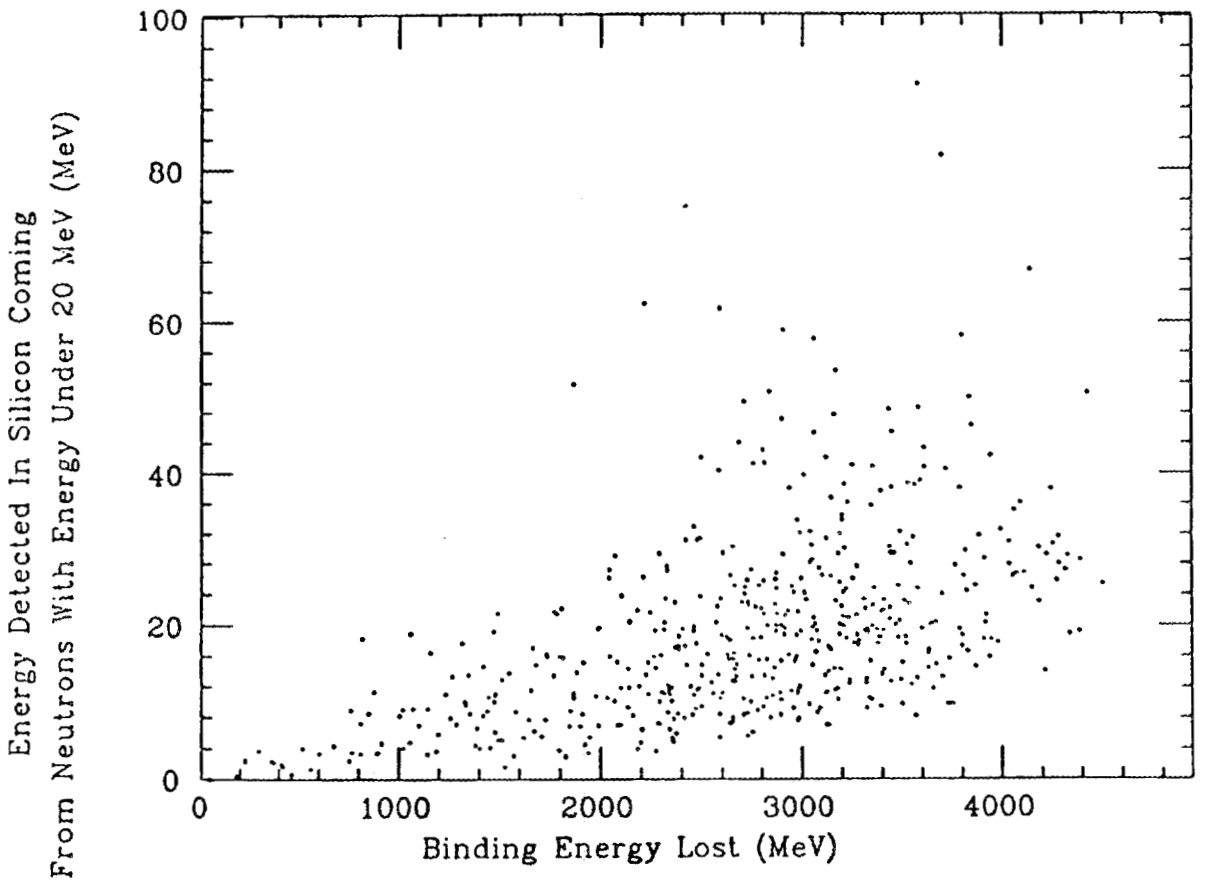

Fig. 14. The correlation of detected low energy (E < 20 MeV) neutron energy in the uranium-silicon calorimeter with the binding energy lost in the hadronic cascade.

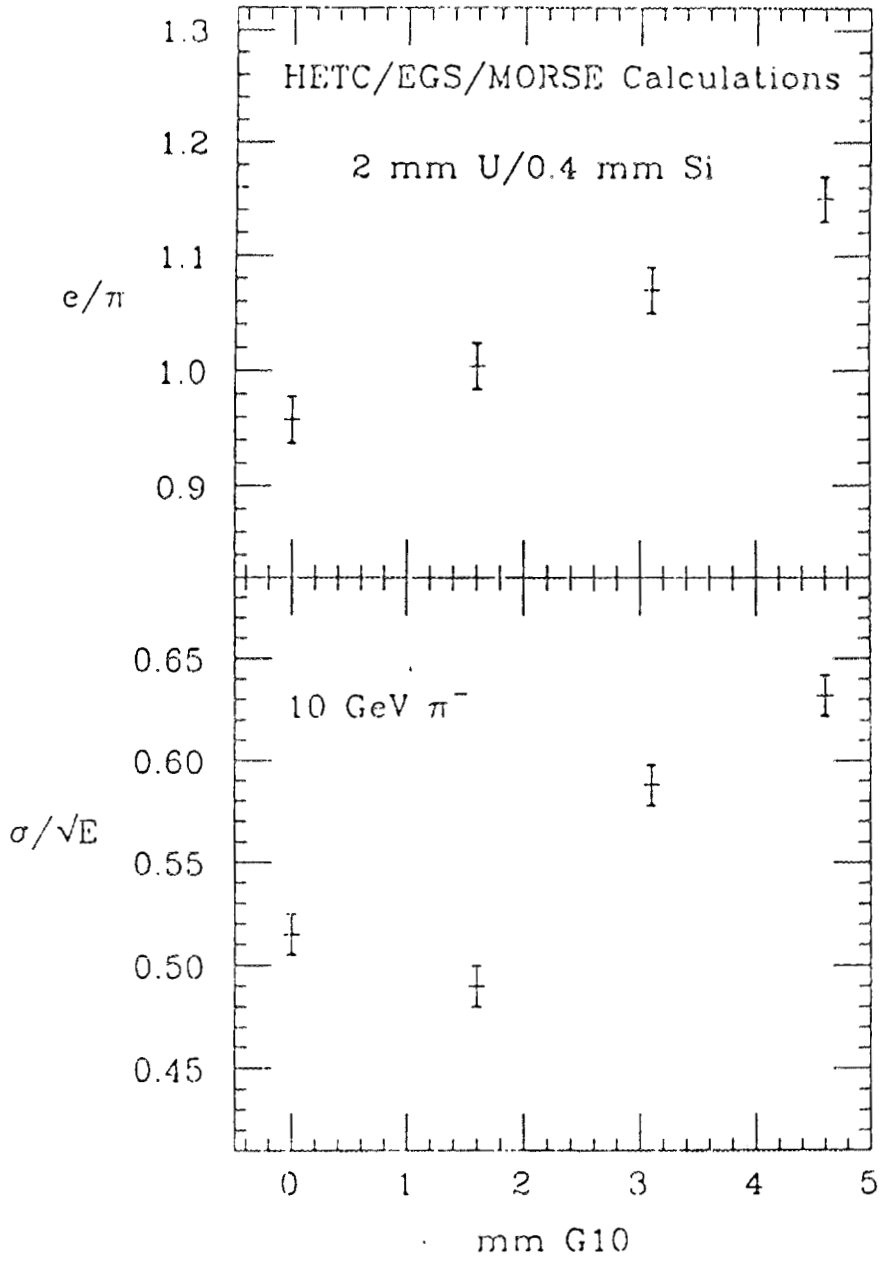

Fig. 15. The calculated variation of e/π and $\sigma/\sqrt{E}$ with the thickness of a G10 sheet placed between the 2 mm uranium plates and the silicon detectors in a uranium-silicon calorimeter for incident 10 GeV π^-. Without G10, a slight overcompensation conditions exists.

radiators, followed by a 1.3 mm air gap, a 1 mm G10 layer, 400 μm of fully depleted silicon, a 1 mm G10 layer, and another 1.3 mm air gap, the e/h ratio increases to 1.29. For the 10 GeV π^- the resolution is $\frac{\sigma}{\sqrt{E}} = 62\%$. Even for the iron, the role of low energy detection efficiency can be seen in the e/h ratio, and for the lead, the e/h ratio of 1.16 is within reach of the values which have been touted as acceptable for future "compensating" calorimeters.[47]

In connection with these calculations, the attractiveness of a low-Z radiator material such are iron should be pointed out. Iron has several advantages compared to uranium, for example. In iron, less binding energy loss in inelastic collisions is realized, and this factor therefore contributes less to the energy spread than in calorimeters employing higher Z radiators. Secondly, connected with this is the fact that fewer neutrons are produced in these collisions and the produced neutrons are a source of radiation damage at high luminosity colliders. Thirdly, uranium is more expensive than iron.[48] Finally, uranium is difficult to obtain and to work with. In spite of these advantages for low Z over high Z, it is difficult to anticipate a practical design of a compensating iron calorimeter. As we have seen, the electromagnetic sampling inefficiencies are an important factor in achieving compensation. These effects are small in iron due to the small value of the charge of the iron nucleus. As a result, the response of an iron calorimeter to electromagnetic and non-electromagnetic energy deposition is much different, yielding large fluctuations in the pulse height distribution. The small binding energy losses are overcome by the fluctuations between electromagnetic and nonelectromagnetic energy. It is conceivable to imagine a combination of low-Z and high-Z material which will combine the advantages of each material and approach a resolution determined by the small binding energy losses of iron.

4. EXPERIMENTAL TEST OF SI/U

The above Monte Carlo studies have predicted compensation in uranium silicon hadron calorimeters. If the experimental results should show that this cannot quite be achieved, further signal-equalization may be obtained with a silicon readout by tuning the electromagnetic component of the hadronic shower.[49–52] The experimental work of the SICAPO Collaboration at CERN is addressing this prospect. A reduction of the energy sensed in electromagnetic showers, caused by the fiberglass (G10) supports of the silicon mosaic, was observed by running the electromagnetic section of a full hadronic calorimeter using uranium absorbers and 0.25 m^2 of silicon active area during 1986.[51] To investigate this observation further, a systematic study of a silicon calorimeter response to electromagnetic shower was performed with small area Si/W and Si/U calorimeters. The measurements were performed at the CERN-PS, with incoming electrons of 2, 4 and 6 GeV, during 1987.[52] Figures 16 and 17 show the mean energy sensed by the calorimeter for Si/W and Si/U respectively, as a function of the incoming electron energy. From these figures it can be seen that in the case of the 5mm G10 absorber (located on the rear side of the detector), the electromagnetic visible energy is reduced by about 29%. The reduction of visible energy (which is energy sensed by the silicon detectors) is greater than the 10% reduction one expected by the addition of the G10 plates.

This 29% reduction in the response of the calorimeter to electromagnetic showers (when 5 mm G10 plates are located on the rear side of the silicon detectors), can be compared to the 10% reduction expected for a purely hadronic shower in the same setup, resulting in a decrease in the value of e/h up to 18%. Thus the compensation condition for Si/U calorimeter is likely to be achieved. On this principle, a perfectly compensating calorimeter of the size needed for LHC/SSC projects is feasible using silicon detectors as active material. The SICAPO collaboration has built a prototype of a Si/U hadronic calorimeter which is 6 interaction lengths deep (Fig. 18). The silicon mosaic active samplers (500 cm^2 active area, but with the possibility to double it as seen in Fig. 19) are located next to 10 mm thick uranium plates. Experimental measurements are expected to start during winter 1988/1989.

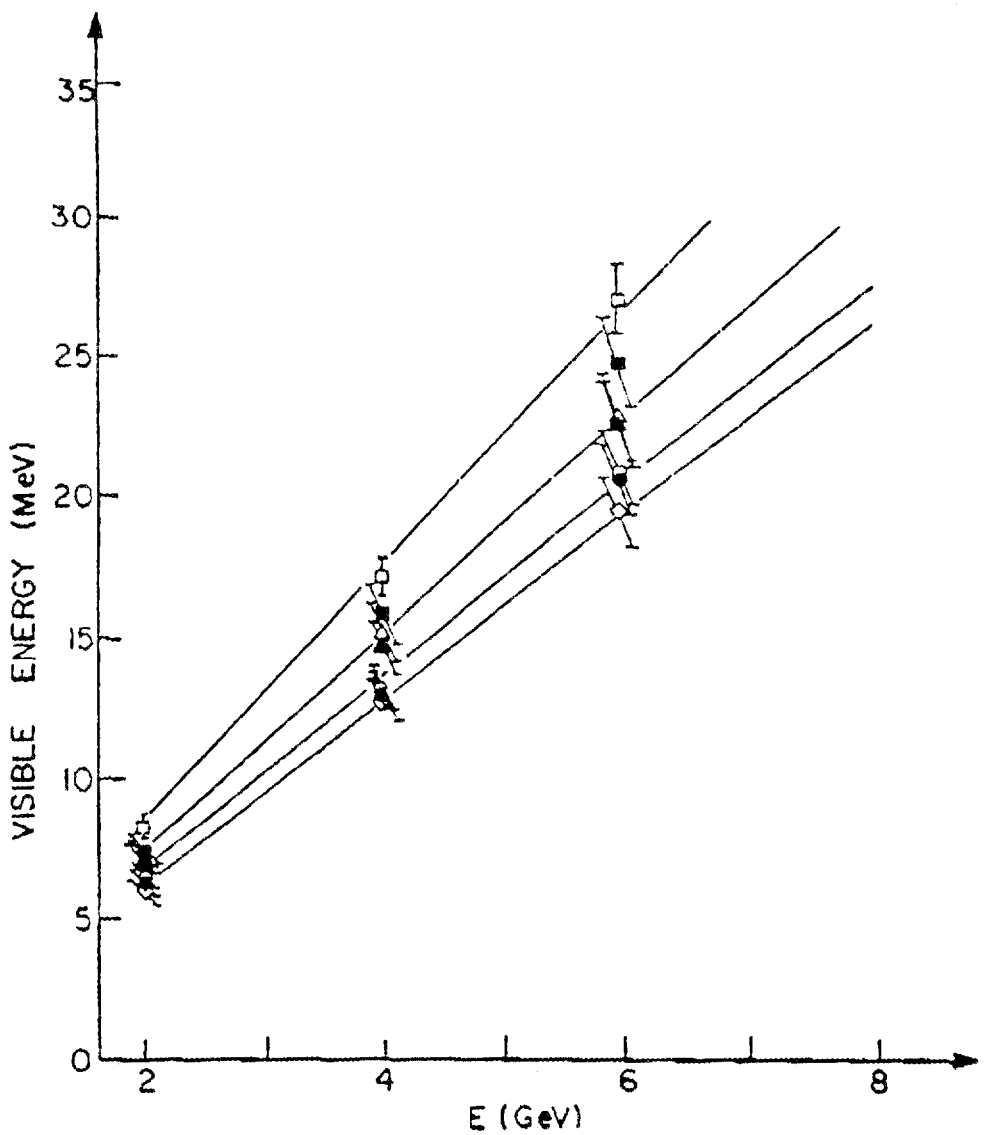

Fig. 16. Mean energy deposited in Si/W calorimeter as a function of the incoming electron energy, from top to bottom:

- □ no absorber in front of detector
- ■ 0.5mm of G10 in front and rear of detectors
- △ 1.0mm of G10 in front and rear of detectors
- ▲ 1.5mm of G10 in front and rear of detectors
- ○ 3.0mm of G10 in front and rear of detectors
- ● 4.0mm of G10 in front and rear of detectors
- ◇ 5.0mm of G10 in front and rear of detectors.

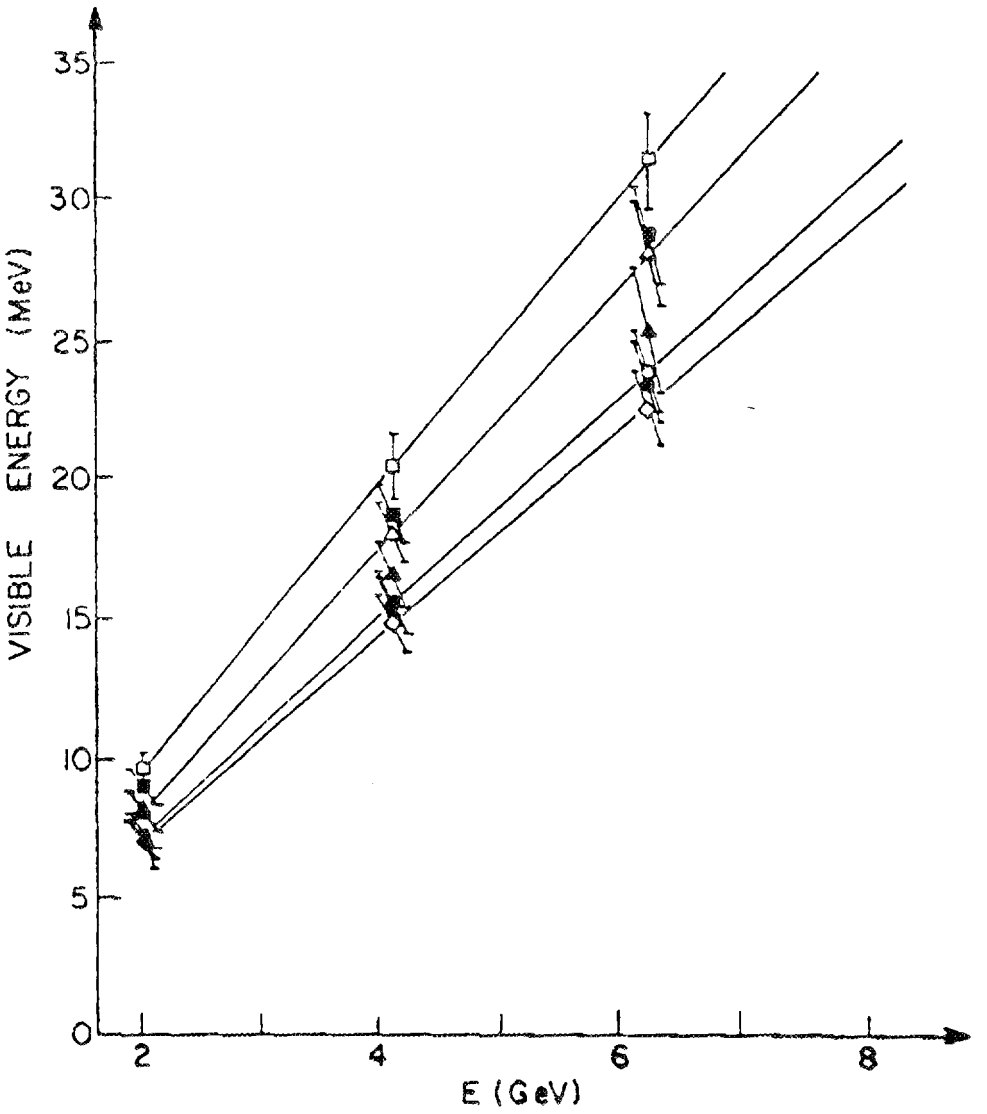

Fig. 17. Mean energy deposited in Si/U calorimeter as a function of incoming electron energy, from top to bottom:

- □ no absorber in front of detector
- ■ 0.5mm of G10 in front and rear of detectors
- △ 1.0mm of G10 in front and rear of detectors
- ▲ 1.5mm of G10 in front and rear of detectors
- ○ 3.0mm of G10 in front and rear of detectors
- ● 4.0mm of G10 in front and rear of detectors
- ◇ 5.0mm of G10 in front and rear of detectors.

Fig. 18. Silicon/U hadronic calorimeter of SICAPO collaboration at CERN PS.

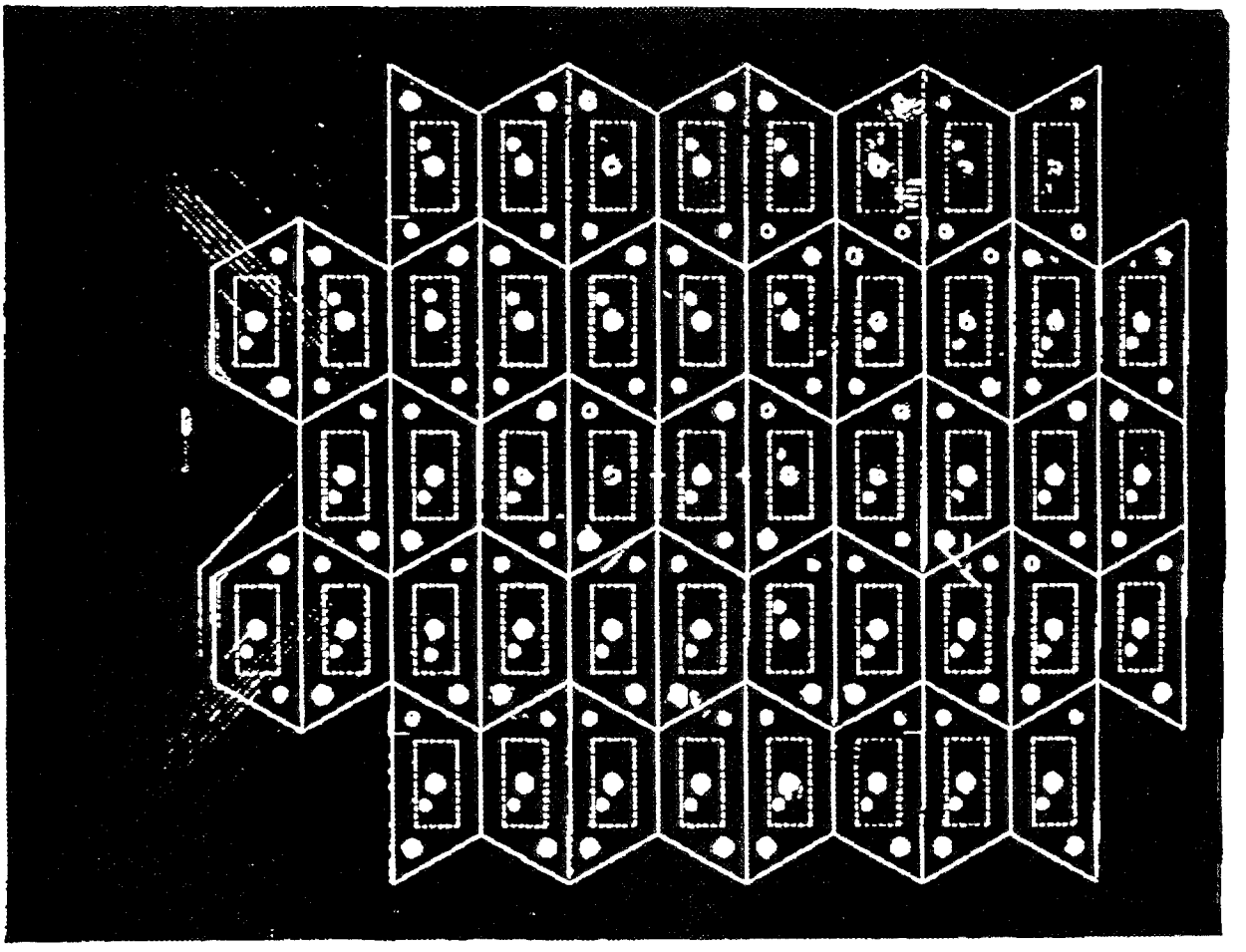

Fig. 19. Silicon mosaic active samplers.

5. DISCUSSION OF POTENTIAL LIMITATIONS

It is important to keep in mind some of the other unsolved problems of silicon readout hadron calorimeters. One very important concern is the tolerance, or potential lack thereof, of silicon to the radiation environment that the future high luminosity, high rate colliders will present. Recent work in this area has illuminated the situation and shown that it is not as dismal as was earlier feared. The improvement in tolerance to neutrons which is expected to occur with higher resistivity materials[53] has been demonstrated.[54] Strong self-annealing effects have been observed following the exposure of such devices to intense neutron sources.[55,56] Finally, a study of the expected effects of the radiation environment of the SSC[20] on the operation of an imagined detector (the compact solenoidal detector) employing silicon calorimeters,[57] including the best understanding of these resistivity dependence effects and self annealing, has concluded that such an operation appears practical.[58] Preliminary results from the SICAPO Collaboration[55] using a DLTS analysis show that the concentration of trapping centers (generated by evaporative neutrons from ^{252}Cf) is negligible with detectors annealing at about 150° C. Further radiation effects tests are called for, but the situation looks manageable.

The second major area of concern is in the cost of providing the detectors for such a project. The total area of silicon required for the calorimeter of the compact solenoidal detector is 20 million cm^2. To make such a project realizable means that devices must be available for about two dollars per cm^2. Presently, devices are being ordered for 6-12 dollars per cm^2 so that an improvement of a factor of 3-6 is needed. The prospects for such an improvement for a detector of the scale of the compact solenoidal detector look good, however.[59]

One final issue of concern must be mentioned and that is the problem of how to read out the detectors while preserving the intrinsic speed. Radeka and Rescia have noted the design constraints on speed for ionization sampling calorimeters.[60] Achieving calorimeter responses of $\sim$20 nanoseconds requires that the product of detector capacitance and inductance of the connections be kept below 4 nsec^2. For a cell of one nanofarad this means the inductance of the connections must be kept below 4 nanoHenries, which requires less than a centimeter of lead for practical means. The compact solenoidal detector design, in fact, proposes about 1 nanofarad per layer of silicon detectors in the hadron calorimeter. Therefore, preserving the intrinsic speed will probably require the mounting of active elements on every layer. While this involves millions of transistors, it appears achievable. The combining of pads in series is also a possible means to achieve reduced capacitance and is being pursued by the SICAPO Collaboration for the prototype silicon-uranium calorimeter. They will be controlling the noise in the experimental program of silicon-iron with detector pads of about 5.5 cm^2 and individual VLSI(BICMOS) preamplifier readouts. Some noise penalty must be accepted to preserve the speed, but it can be sufficiently limited by these procedures. This may prevent calibration of the calorimeter with muons, but shouldn't limit the energy resolution of real physics signatures.

6. CONCLUSIONS

The new understanding of compensating calorimeters which was introduced four years ago has now been experimentally confirmed in numerous tests. One important element of that understanding was the role of saturation in uranium-liquid argon calorimeters. High rate, high energy colliders are going to demand compensating, fast, finely segmented calorimeters. The calculations presented here indicate that the near absence of saturation in silicon should lead to compensation. Silicon's other attractive features (speed, ease of segmentation, and absolute gain calibration) make it an extremely attractive approach. An experimental program by the SICAPO Collaboration is underway at CERN to test these expectations.

APPENDIX

THE METHOD OF CALCULATION

The calculations reported here have been performed with the CALOR computer code system following approximately the procedures used in previous calculations.[61,31,7,8] The three-dimensional, multimedia, high-energy nucleon-meson transport code HETC[62] was used, with modifications to obtain a detailed description of the nucleon-meson cascade produced in the devices considered in this paper. The source distribution for the electromagnetic cascade calculation is provided by HETC. The transport of the electrons, positrons, and gammas from these sources is carried out using the EGS system.[41] Neutrons which are produced with energies below 20 MeV are transported using the MORSE[63,64] Monte Carlo transport code. Gamma rays (including those from capture, fission, etc.) produced during this phase of the calculations are stored for transport by the EGS code. The nonlinearity of the light pulse or charge collected (L) due to saturation effects is taken into account by the use of Birks' law:[37]

$$\frac{dL}{dx} = \frac{S\frac{dE}{dx}}{1 + kB\frac{dE}{dx}}, \tag{3}$$

where kB is the saturation constant. Further details of these calculations can be found in the Appendix of Ref. 32.

REFERENCES

1. S. Iwata, Nagoya University Report,DPNU-3-79 (1979)
2. U. Amaldi, Phys. Scripta 23, 409 (1981)
3. C.W. Fabjan and T. Ludlam, Ann. Rev. Nucl. Part. Sci. 32, 335 (1982)
4. C.W. Fabjan, CERN-EP/85-54 (1985)
5. J.E. Brau and T.A. Gabriel, SLD-New Detector Note No. 119, May 22, 1984
6. J.E. Brau, Proceedings of the September 1984 Seattle meeting of the SLD Collaboration
7. J. Brau and T.A. Gabriel, Nucl. Instrum. and Methods A238, 489 (1985)
8. T.A. Gabriel, B.L. Bishop, J. Brau, A. DiCiaccio, M. Goodman, and R. Wilson, IEEE Trans. Nucl. Sci. NS-32, 1 (1985)
9. J. E. Brau, Proc. Workshop on Compensated Calorimetry, Pasedena (1985) CALT-68-1305
10. T.A. Gabriel, Proc. Workshop on Compensated Calorimetry, Pasedena (1985) CALT-68-1305
11. P.M. Mockett, Proceedings of the Eleventh SLAC Summer Institute on Particle Physics, July 1983, ed. Patricia M. McDonough, SLAC-267 (1984)
12. H. Gordon and P. Grannis, Proceedings of the 1984 Summer Study on the Design and Utilization of the SSC, Snowmass, Colorado, p. 591 (1984), eds. R. Donaldson and J.G. Morfin
13. H. Brückmann, Proc. Workshop on Compensated Calorimetry, Pasedena (1985) CALT-68-1305
14. G. d'Agostini et al, NIKHEF-H/88-4 (April 1988)
15. E. Bernardi et al, Nucl. Instrum. and Methods A262, 229 (1987)
16. C. Leroy, Y. Sirois, and R. Wigmans, Nucl. Instrum. and Methods A252, 4 (1986)
17. R. Wigmans, Nucl. Instrum. and Methods A259, 389 (1987)
18. H. Brückmann et al, Nucl. Instrum. and Methods A263, 136 (1988)
19. D. Soper, presentation at the Workshop on Experiments, Detectors, and Experimental Areas for the Supercollider, Berkeley, California, 1987
20. D. Groom (ed.), SSC-SR-1033 (1988)
21. T. Kondo, Y. Watanabe, and S. Kim, Proceedings of the 1984 Summer Study on the Design and Utilization of the SSC, Snowmass, Colorado, p. 612 (1984), eds. R. Donaldson and J.G. Morfin
22. P.G. Rancoita and A. Seidman, Nucl. Instrum. and Methods A263, 84(1988); S. Pensotti, P.G. Rancoita, A.Seidman, and L. Vismara, Nucl. Instrum. and Methods A265, 266(1988)

23. G. Barbiellini et al, Nucl. Instrum. and Methods A235, 55(1985); G. Barbiellini et al, Nucl. Instrum. and Methods A236, 316 (1985); M. Bormann et al, Nucl. Instrum. and Methods A240, 63 (1985); and A. Nakamoto et al, Nucl. Instrum. and Methods A251, 275 (1985)

24. T. Akesson et al, CERN-EP/87-88

25. SICAPO Collaboration, presented by C. Leroy and F. Lemeilleur, International Conference on Advanced Technology and Particle Physics, Villa Olmo, Lake Como, Italy, June, 1988

26. C.W. Fabjan et al, Nucl. Instrum. and Methods 141, 61 (1977)

27. T.A. Gabriel, ORNL/TM-9727 (1985)

28. G. Rudstam, Z. Naturforsch. 21a,1027 (1966); G. Rudstam, Nucl. Phys. A126, 401 (1969)

29. This count does not include neutron nuclear collisions for neutrons below 20 MeV

30. Note that the prompt gammas mentioned above, although ineffective, are included in the calculations described here

31. T.A. Gabriel, Nucl. Inst. and Methods 150, 145 (1978)

32. J.E. Brau and T.A. Gabriel, International Conference on Advanced Technology and Particle Physics, Villa Olmo, Lake Como, Italy, June, 1988 (to be published in Nuclear Instruments and Methods.)

33. J.E. Brau and T.A. Gabriel, Appendix 15 of SSC-SR-1033, edited by D. Groom (1988)

34. O. Botner et al, IEEE Trans. Nucl. Sci. NS-28, 510 (1981); O. Botner et al, Nucl Inst. and Methods 179, 145 (1981)

35. P. Rehak, Proc. Workshop on Compensated Calorimetry, Pasedena (1985) CALT-68-1305

36. G. Knoll, Radiation Detection and Measurement, John Wiley and Sons, New York (1979), p. 570

37. J.Birks, Proc. Phys. Soc. A64, 874 (1951)

38. W. Hofmann et al, Nucl. Inst. and Methods 135, 151 (1976)

39. This value calculated for this calorimeter represents the lowest obtainable value for e/h. Note that liquid argon could be made to compensate if a method were available to retrieve all of the deposited energy

40. J.H. Hubbell, Int. J. Appl. Radiat. Isot. 33, 1269 (1982); J.H. Hubbell, H.A. Gimm, and I. Overbo, J. Phys. Chem. Ref. Data 9, 1023 (1980); E. Storm and H.I. Israel, Nucl. Data Tables A7, 565 (1970)

41. R.L. Ford and W.R. Nelson, SLAC-0210 (1978)

42. B.D. Wilkins, M.J. Fluss, S.B. Kaufman, C.E. Gross, and E.P. Steinberg, Nucl. Instrum. and Methods 92, 381 (1971)

43. A.R. Sattler, Phys. Rev. 138, A1815 (1965)

44. D. I. Garber and R.R. Kinsey, BNL 325 (1976)

45. It is emphasized that the e/h ratio was calculated assuming no saturation in the silicon

46. T.A. Gabriel, J.O. Johnson, and J.E. Brau, Proceedings of the Workshop on Detector Simulation for the SSC, Argonne National Laboratory, August, 1987

47. M.G.D. Gilchriese, Proceedings of the 1987 SLAC Summer Institute on Particle Physics

48. C. Baltay, J. Huston, and B.G. Pope, Proceedings of the 1986 Summer Study on the Physics of the Superconducting Supercollider, Snowmass, Colorado, p. 355 (1986), eds. R. Donaldson and J. Marx

49. S. Pensotti, P.G. Rancoita, A. Seidman and L. Vismara, Nucl. Instrum. and Methods, A265, 266 (1988)

50. C. Furetta, S. Pensotti, P.G. Rancoita, L. Vismara, G. Barbiellini and A. Seidman, IEEE Trans. Nucl. Sci., 35, 446 (1988)

51. S. Pensotti, P.G. Rancoita, C. Simeone, L. Vismara, G. Barbiellini and A. Seidman, Nucl. Instrum. and Methods, A270, 327 (1988)

52. SICAPO Collaboration to be submitted for publication in Phys. Lett. B

53. G.C. Messenger and M.S. Ash, The Effects of Radiation on Electronic Systems, Van Nostrand Reinhold, New York, (1986), p. 157

54. H.W. Kraner, Z. Li, M. Momayezi, and K. Posnecker, International Conference on Advanced Technology and Particle Physics, Villa Olmo, Lake Como, Italy, June, 1988

55. SICAPO Collaboration, presented by L. Vismara, International Conference on Advanced Technology and Particle Physics, Villa Olmo, Lake Como, Italy, June, 1988

56. T. Kondo and T. Ohsugi, private communication

57. J. Kirkby, T. Kondo, S.L. Olsen et al, Proceedings of the Workshop on Experiments, Detectors, and Experimental Areas for the Supercollider, Berkeley, California, p. 388 (1988), eds. R. Donaldson and M.G.D. Gilchriese

58. T. Ohsugi, H.Ikeda, and T. Kondo, Appendix 4 of SSC-SR-1035, edited by M.G.D. Gilchriese (1988)

59. Private discussions with industry

60. V. Radeka and S. Rescia, Nucl. Instrum. and Methods A265, 228 (1988)

61. T. A. Gabriel and W. Schmidt, Nucl. Instr. and Meth. 134, 271(1976)

62. K. C. Chandler and T. W. Armstrong, Oak Ridge National Laboratory, ORNL-4744 (1972); H. W. Bertini, Phys. Rev. 188, 1711(1969)

63. M. B. Emmett, Oak Ridge National Laboratory, ORNL-4972, (1975)

64. N. M. Greene et al., Oak Ridge National Laboratory, ORNL/TM-3706, (1973)

INTERNAL DISTRIBUTION

1. F. S. Alsmiller
2. R. G. Alsmiller, Jr.
3. B. R. Appleton
4. D. E. Bartine
5. B. L. Bishop
6–10. T. A. Gabriel
11. J. K. Ingersoll
12. R. A. Lillie
13. F. C. Maienschein
14. RSIC
15. C. Zeigler
16. EPMD Reports Office
17–18. Laboratory Records Department
19. Laboratory Records, ORNL-RC
20. Document Reference Section
21. Central Research Library
22. ORNL Patent Section

EXTERNAL DISTRIBUTION

23. Office of the Assistant Manager for Energy Research and Development, Department of Energy, Oak Ridge Operations, P.O. Box 2001, Oak Ridge, TN 37831
24–33. Office of Scientific and Technical Information, PO Box 62, Oak Ridge, TN 37830
34. Argonne National Laboratory, Library Services Dept., 302-CE125, 9700 S. Cass Avenue, Argonne, IL 60439
35. T. W. Armstrong, Science Applications, Inc., PO Box 2807, La Jolla, CA 92038
36. Miguel Awschalom, National Accelerator Laboratory, PO Box 500, Batavia, IL 60510
37. V. S. Barashenkov, Laboratory of Theoretical Physics, Joint Institute for Nuclear Research, Head Post Office, PO Box 79, Moscow, USSR
38. Gerald W. Bennett, Brookhaven National Laboratory, Upton, NY 19973
39. D. Berley, National Science Foundation, Washington, DC 20550
40. Elliott Bloom, Stanford Linear Accelerator Center, PO Box 4349, Stanford, CA 94305
41. J. Brau, University of Oregon, Eugene, OR 97403
42. Bruce Brown, Fermi National Accelerator Laboratory, PO Box 500, Batavia, IL 60510
43. David O. Caldwell, Dept. of Physics, University of California at Santa Barbara, Santa Barbara, CA 93106
44. Stanley B. Curtis, Lawrence Radiation Laboratory, Bldg. 29, Room 213, Berkeley, CA 94720
45. Herbert DeStaebler, Stanford Linear Accelerator Center, Stanford University, Stanford, CA 94305
46. Tom Dombeck, Division of High Energy & Nucl. Phys., U.S. Department of Energy, Washington, DC 20874
47. A. Di Ciaccio, CERN, Geneva 23, Switzerland
48. J. J. Dorning, Dept. of Nucl. Eng. and Engineering Physics, University of Virginia, Charlottesville, VA 22901
49. R. D. Edge, Physics Dept., University of South Carolina, Columbia, SC, 29208
50. R. Eisenstein, Dept. of Physics, University of Illinois, Urbana, IL 61801

51. R. W. Ellsworth, George Mason University, Fairfax, VA 22030
52. Chris Fabjan, CERN, Geneva 23, Switzerland
53. G. Feldman, Stanford Linear Accelerator Center, Stanford University, Stanford, CA 94305
54. W. T. Ford, Experiment 1A-Lab C, Fermi National Accelerator Laboratory, PO Box 500, Batavia, IL 60510
55. E. Fowler, Dept. of Physics, Purdue University, West Lafayette, IN 47907
56. H. T. Freudenreich, University of Maryland, College Park, MD 20742
57. E. Freytag, Deutsches Elektronen-Synchrotron, DESY, 2 Hamburg Dr., Flottbek, Notkesteig 1, W. Germany
58. A. F. Garkinkel, Purdue University, Dept. of Physics, West Lafayette, IN 47907
59. M. G. D. Gilchriese, SSC Central Design Group, Lawrence Berkeley Laboratory, Berkeley, CA 94720
60. G. T. Gillies, Dept. of Physics, University of Virginia, Charlottesville, VA 22901
61. G. E. Gladding, University of Illinois, Dept. of Physics, Urbana, IL 61801
62. K. Goebel, Health Physics Group, CERN, 1211 Geneva 23, Switzerland
63. J. A. Goodman, University of Maryland, College Park, MD 20742
64. M. Goodman, Bell Communication Research, Morristown, NJ 07960
65. D. Groom, SSC Central Design Group, Lawrence Berkeley Laboratory, Berkeley, CA 94720
66. Herman Grunder, Deputy Director, General Sciences, Lawrence Berkeley Laboratory, Bldg. 50A, Room 4119, 1 Cyclotron Rd., Berkeley, CA 94720
67. H. J. Hargis, University of Tennessee, Dept. of Physics, Knoxville, TN 37919
68. Frenc Hajnal, Health and Safety Laboratory, U.S. Department of Energy, 376 Hudson St., New York, NY 120014
69. R. M. Haralick, Dept. of Electrical Engineering, University of Washington, Seattle, WA 98195
70. M. Hofert, CERN, 1211 Geneva 23, Switzerland
71. Terrence Jensen, Dept. of Physics and Astronomy, The University of Rochester, Rochester, NY 14627
72. D. Lal, Tata Institute of Fundamental Research, National Centre of the Government of India, for Nuclear Science & Mathematics, Homi Bhabha Rd.,, Bombay 5, India
73. Lawrence Livermore Laboratory, Technical Information Department, PO Box 808, Livermore, CA 94550
74. V. Lebedev, Institute of High Energy Physics, Serpukhov, Moscow Region, USSR
75. Library for Nuclear Science, Massachusetts Institute of Technology at Middleton, Middleton, MA 01949
76. J. LoSecco, Dept of Physics, California Institute of Technology, Pasadena, CA 91125
77. J. Marks, Accelerator Fusion Research Division, Lawrence Berkeley Laboratory, Bldg. 50, Room 149, 1 Cyclotron Rd., Berkeley, CA 94720
78. A. I. Mincer, University of Maryland, College Park, Md 20742
79. V. S. Narashimham, Tata Institue of Fundamental Research, Bombay 400 005,, India
80. W. R. Nelson, Stanford Linear Acclerator Center, Stanford University, PO Box 4349, Stanford, CA 94305

81. T. R. Palfrey, Jr., Dept. of Physics, Purdue University, West Lafayette, IN 47907
82. Robert Palmer, Brookhaven National Laboratory, Upton, NY 11973
83. C. W. Peck, Dept. of Physics, California Institute of Technology, Pasadena, CA 91109
84. J. Ranft, Karl-Marx University, Physics Section, Linnestrasse 5, 701, Leipzig, E. Germany
85. Lincoln Read, Division of High Energy & Nuclear Physics, Department of Energy, Washington, DC 20545
86. Jim Reidy, University of Mississippi, University, MS 38677
87. Enloe T. Ritter, Div. of High Energy & Nucl. Phys., ER-221, U.S. Department of Energy, 19901 Germantown Rd., Germantown, MD 20874
88. C. Rubbia, Lyman Laboratory, Harvard University, Cambridge, MA 02138
89. W. Schmidt, Institute of Experimental Nuclear Physics, University of Karlsruhe, 75 Karlsruhe, W. Germany
90. The Secretary, Radiation Group, Lab II, CERN, 1211 Geneva 23, Switzerland
91. Walter Selove, University of Pennsylvania, Dept. of Physics, Philadelphia, PA 19104
92. B.S.P. Shen, Dept. of Astronomy, University of Pennsylvania, Philadelphia, PA 19104
93. M. Shupe, Dept. of Physics, University of Minnesota, Minneapolis, MN 55455
94. Alan Stevens, Physics Dept., Brookhaven National Laboratory, Upton, NY 11973
95. G. R. Stevenson, Radiation Protection Group, Lab II, CERN, 1211 Geneva 23, Switzerland
96. L. Sulak, Dept. of Physics, University of Michigan, Ann Arbor, MI 48109
97. R. F. Taschek, Los Alamos National Laboratory, PO Box 1663, Los Alamos, NM 87544
98. R. Tesch, DESY, Hamburg, Notkesteig 1, W. Germany
99. R. H. Thomas, Lawrence Radiation Laboratory, Health Physics Dept., Bldg. 72, Berkeley, CA 94720
100. V. D. Toneev, Laboratory of Theoretical Physics, Joint Institute for Nuclear Research, Head Post Office, PO Box 79, Moscow, USSR
101. S. C. Tonwar, University of Maryland, College Park, Md 20742
102. W. Turchinetz, Massachusetts Institute of Technology, R26-411, Cambridge, MA 02139
103. Jim Walker, University of Florida, Gainesville, FL 32611
104. W. J. Willis, CERN, Geneva 23, Switzerland
105. D. Winn, Lyman Laboratory, Harvard University, Cambridge, MA 02138
106. J. Wilczynski, Nuclear Research Center, Karlsruhe, W. Germany
107. S. Yellin, Stanford University, Stanford Linear Accelerator Center, PO Box 4349, Stanford, CA 94305
108. G. B. Yodh, University of Maryland, College Park, MD 20742
109. S. Youssef, SCRI, Florida State University, Tallahassee, FL 32306
110. B. Zeitnitz, Nuclear Research Center, Karlsruhe, W. Germany